PLOS BIOLOGY

Anticipation-induced delta phase reset improves human olfactory perception

Ghazaleh Arabkheradmand[1], **Guangyu Zhou**[1]*, **Torben Noto**[1], **Qiaohan Yang**[1], **Stephan U. Schuele**[1], **Josef Parvizi**[2], **Jay A. Gottfried**[3,4], **Shasha Wu**[5], **Joshua M. Rosenow**[6], **Mohamad Z. Koubeissi**[7], **Gregory Lane**[1], **Christina Zelano**[1]

1 Northwestern University Feinberg School of Medicine, Department of Neurology, Chicago, Illinois, United States of America, **2** Laboratory of Behavioral and Cognitive Neuroscience, Department of Neurology and Neurological Sciences, Stanford University Palo Alto, Stanford, California, United States of America, **3** University of Pennsylvania, Perelman School of Medicine, Department of Neurology, Philadelphia, Pennsylvania, United States of America, **4** University of Pennsylvania, School of Arts and Sciences, Department of Psychology, Philadelphia, Pennsylvania, United States of America, **5** University of Chicago, Department of Neurology, Chicago, Illinois, United States of America, **6** Northwestern University Feinberg School of Medicine, Department of Neurosurgery, Illinois, United States of America, **7** George Washington University, Department of Neurology, Washington DC, United States of America

* guangyu.zhou@northwestern.edu

Abstract

Anticipating an odor improves detection and perception, yet the underlying neural mechanisms of olfactory anticipation are not well understood. In this study, we used human intracranial electroencephalography (iEEG) to show that anticipation resets the phase of delta oscillations in piriform cortex prior to odor arrival. Anticipatory phase reset correlates with ensuing odor-evoked theta power and improvements in perceptual accuracy. These effects were consistently present in each individual subject and were not driven by potential confounds of pre-inhale motor preparation or power changes. Together, these findings suggest that states of anticipation enhance olfactory perception through phase resetting of delta oscillations in piriform cortex.

Introduction

Anticipation enhances sensory perception by improving stimulus detection and discrimination [1–8]. Anticipation-driven sensory enhancements can be dramatic in the human olfactory system, where detection thresholds of an anticipated smell may be significantly lower than thresholds for the spontaneous—that is, unanticipated—detection of the same odor. For example, industry standards of warning odorant concentration, such as the addition of ethyl-mercaptan to natural gas, can require a 57,000-fold increase in concentration over attended detection thresholds [9]. Yet the mechanism by which olfactory anticipation enhances perception is not well understood. In the visual and auditory systems, anticipation may impact perception through modulation of the excitability of local neuronal populations in sensory cortex [10–19] or through resetting of the phase of ongoing local field potential (LFP) oscillations prior to stimulus arrival [20–46]. Whether similar effects occur in the human olfactory system,

Abbreviations: BOLD, blood oxygen level dependent; CT, computed tomography; DMP, deviation from the mean phase; FDR, false discovery rate; fMRI, functional magnetic resonance imaging; ITPC, intertrial phase coherence; iEEG, intracranial electroencephalography; LFP, local field potential; MNI, Montreal Neurological Institute; MRI, magnetic resonance imaging; PSD, power spectral density.

with its phylogenetically older architecture and unique thalamic organization, is unknown. Though decades of research have focused on behavioral and neural correlates of attention in the visual and auditory systems [47–51], olfactory attention is far less studied.

Humans are capable of bringing selective attention to olfaction, which increases response speeds and impacts sniffing behavior [52–54]. Furthermore, olfactory attention modulates odor-evoked activity in the human brain [55–58], specifically in olfactory cortex [52,59–63]. Though fewer olfactory attention studies have focused on anticipation prior to the arrival of odor, enhanced functional magnetic resonance imaging (fMRI) signals have been observed prior to the onset of an odor in olfactory cortex, during anticipation [60,64]. However, fMRI measures of blood oxygen level dependent (BOLD) signals are unable to measure increases in excitability and phase synchrony within local neural populations. Thus, the oscillatory dynamics underlying olfactory anticipatory states are not well understood in the human brain. Olfactory attention also occurs in rodents, in whom it improves olfactory response times and thresholds [65–67]. A recent pioneering study showed that rats are capable of olfactory selective attention and that olfactory attentive and anticipatory states sharpen single-unit responses in the olfactory tubercle, resulting in increased stimulus contrast [66]. However, the importance of oscillatory phase dynamics—which have been shown to be critical during anticipation in other sensory systems—remain unclear in the olfactory system.

Numerous studies have established that LFP oscillatory dynamics are fundamental to olfactory processing mechanisms [68–83]. In rodents and humans, LFP oscillations in the olfactory bulb and in piriform cortex align to respiration [68,73,77,80,84–93], reflecting the fact that olfactory sampling is tied to breathing. Inhaling always brings with it the possibility of encountering an odor. In fact, the olfactory system allows fine control over the timing of an anticipated odor, through timing of the nasal inhale, which delivers odor molecules to receptors in the nose. Therefore, an investigation into the role of LFP oscillatory dynamics in olfactory anticipation will necessarily involve consideration of the relationship between those dynamics and the onset of inhalation, which is linked to the onset of odor.

We hypothesized that despite architectural and organizational differences between olfactory and other sensory systems [94], LFP phase would reset prior to inhalation onset—that is, stimulus onset—in the olfactory system, as is the case in other sensory systems. This would suggest that phase resetting as a neural signature of sensory anticipation is preserved across sensory systems of varied phylogenetic age and that the olfactory system is capable of similar mechanisms even without the precortical thalamic relay, which may be critical for these mechanisms in other modalities [1,30].

In this study, we used intracranial electroencephalography (iEEG) recordings from human piriform cortex (Fig 1A) to study the neural signatures of olfactory anticipation in the human olfactory system. Using iEEG, we were able to record LFPs with high temporal precision, allowing us to test the hypothesis that anticipation of odor would reset the phase of LFP oscillations in piriform cortex prior to inhale onset. We further hypothesized that if this phase reset was related to anticipation-induced enhancement of perception, then it would predict the strength and accuracy of subsequent neural and behavioral responses to the ensuing odor.

Results

We investigated olfactory anticipation in a set of data gathered from neurosurgical patients with intracranial electrodes in piriform cortex who participated in olfactory tasks over the last 10 years, selected by inclusionary criteria (Fig 1B). This selection took advantage of the fact that most human olfactory tasks involve periodic, cued trials including presentation of odors, separated by fairly large intertrial intervals, during which participants breathe without
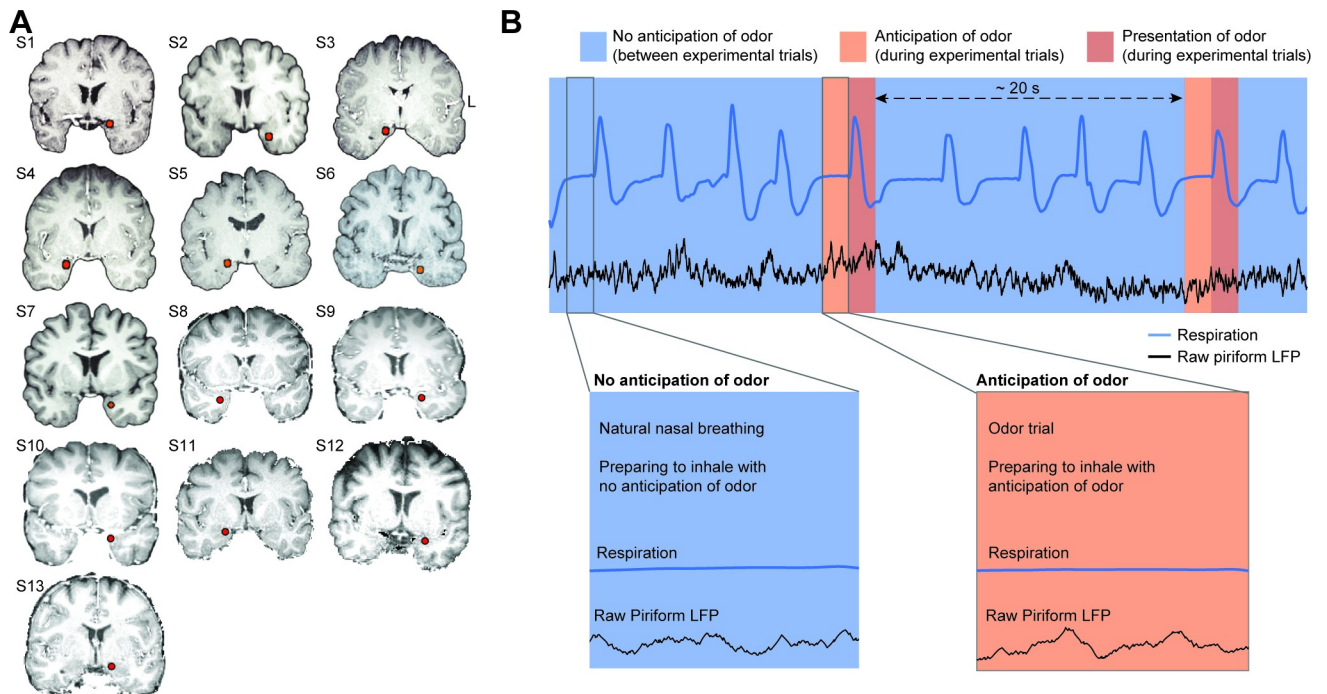
Fig 1. Electrode locations and experimental conditions. (A) The location of the piriform cortex electrode (red dot) is shown on each participant's brain image. L, left hemisphere. (B) Schematic illustration of anticipatory and nonanticipatory conditions. Inhales taken in anticipation of odor (during experimental trials) were compared to inhales taken without anticipation of odor (between experimental trials). Magnified panels show time windows of interest, which included the 1 s time window prior to inhale. Our analyses focused on the time just prior to inhale, when the subject was either anticipating or not anticipating an odor. LFP, local field potential.

anticipation of odor. Thus, data obtained from a typical olfactory task includes nasal inhalations taken in anticipation of an odor (experimental trials) and nasal inhalations taken without anticipation of odor (nasal inhalations taken between trials). We focused on the time windows just prior to these two types of inhalations, which constituted the two conditions of interest for this study—anticipatory and nonanticipatory. Inclusionary criteria were defined by the following considerations: In order to maintain a clear distinction between anticipatory and nonanticipatory inhalations, the time between trials must be adequately long; in order to test for the effects of anticipation on the ensuing olfactory coding, trials must include performance of a perceptual task; and finally, in order to precisely compare conditions, inhale onsets during both the trial and nontrial periods must be clear in the respiratory data. We therefore reviewed all of our olfactory iEEG data sets collected since 2010 in order to identify those which met these criteria: (1) human neurosurgery participants were periodically presented with cued odors, (2) the time between odor presentations exceeded 6 times the respiratory period of the individual, (3) participants performed an olfactory perceptive task, and (4) respiratory data were consistently of high enough quality to accurately determine inhale onsets both during and between trials. We identified data sets from 21 neurosurgical participants performing olfactory tasks, and, with our restrictions, 8 were excluded, leaving 13 participants who met our criteria and were included in the study (Fig 1A).

In each data set, we analyzed the time window just prior to nasal inhalations taken both with and without anticipation of odor (Fig 1B). In order to isolate the effects of anticipation from respiration or odor processing, we focused on a time period when subjects were engaged in a natural pause between breaths—neither inhaling nor exhaling—and on the verge of taking

their next breath, prior to any odor onset. Focusing on the pre-inhale time window ensured a highly controlled experimental comparison by allowing consideration of the effects of anticipation in the absence of sniffing behavior and in the absence of odor—two parameters which could potentially confound interpretation of results. Therefore, the only difference between conditions was whether the ensuing inhale would be taken with anticipation of an odor or without anticipation of an odor (Fig 1B).

Anticipation resets the phase of human piriform oscillations

When attention is brought to odor—for example, when opening the lid of a cooking pot to smell its contents—humans enter into a deliberate state of anticipation just prior to nasal inhalation. Here, we tested the hypothesis that anticipation of odor resets the phase of LFP oscillations in human piriform cortex just prior to anticipatory inhalation. Previous studies in the visual and auditory systems have found a particular importance of delta range oscillations (0–3 Hz) in anticipatory mechanisms in humans and monkeys [21,32,35,39,95]. Therefore, we expected to find anticipatory phase resetting in the human olfactory system mainly at low frequencies. To test this hypothesis, we compared the phase coherence of oscillations prior to inhale onset across anticipatory trials (anticipatory condition) with phase coherence across nonanticipatory trials (nonanticipatory condition). We used Intertrial Phase Coherence (ITPC), which measures the consistency of instantaneous phase values over event-locked trials [96–98] to estimate phase resetting [32,98]. We first created inhale-onset-aligned epochs of anticipatory and nonanticipatory trials for each participant. We then computed the ITPC across a broad range of frequencies (0.5–200 Hz) and times (1 s prior to inhale onset to 3 s following). We found that just prior to anticipatory inhales, statistically significant ITPC was evident in the low-frequency range (0.5–1.5 Hz; Fig 2A and 2B, right). Just prior to nonanticipatory inhales, no ITPC was evident (Fig 2A and 2B, left). In a direct statistical comparison between the two, anticipatory ITPC was significantly stronger than nonanticipatory ITPC in the low-frequency range. Importantly, this effect was evident in both a combined analysis, including data from all trials across all participants (permutation test, false discovery rate [FDR] corrected $P < 0.05$; max $Z = 4.38$), and at the individual level, with significant increases evident in each participant (two-tailed paired t test, $T_{12} = 3.62$, $P = 0.0035$; Figs 2C and 3A). The effect was specific to piriform cortex, with reduced ITPC values in electrodes located outside of piriform cortex on the same implanted depth wire (two-tailed paired t test, $T_{12} = 2.37$, $P = 0.035$; Fig 2E). Though statistically significant ITPC was also evident at higher frequencies, there were no significant differences between conditions; this suggests that while higher frequency oscillations (across a broad range of beta and gamma bands) do align with inhalation, the phase clustering at these frequencies may not be modulated by anticipation.

In the combined analysis, it was evident that the increase in low-frequency phase coherence preceding anticipatory inhales began approximately 0.5 s prior to inhale onset (Fig 2A and 2B). To determine whether the timing of ITPC was consistent across participants, we divided the pre-inhale time window into two separate intervals: [−1 s, −0.5 s] and [−0.5 s, 0 s] prior to inhale onset. We then computed maximal low-frequency (0.5–2 Hz) ITPC values within each time interval for each participant separately. In a two-way repeated ANOVA computed with "anticipatory-state" and "time-window" as factors, we found that, overall, ITPC was significantly stronger in the anticipatory compared to nonanticipatory condition (main effect of anticipatory-state: $F_{1,12} = 12.53$, $P = 0.0041$; Fig 2D). This difference was statistically more significant in the later time interval, beginning 0.5 s prior to inhale onset, evidenced by a significant interaction between anticipatory-state and time-window factors ($F_{1,12} = 13.56$, $P = 0.0031$). This effect was further evidenced by a direct comparison of individual
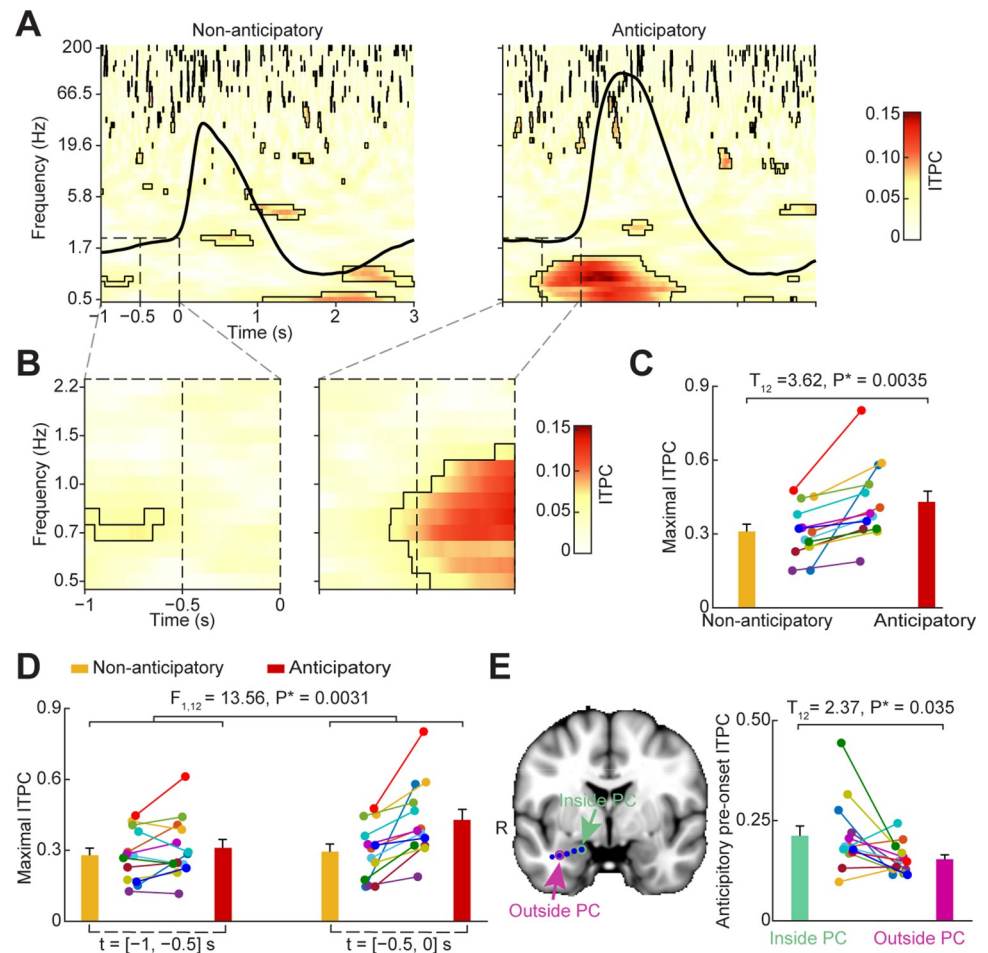
Fig 2. Anticipation of odor induces phase reset prior to inhale. (A) Time-frequency plot of phase reset. The t = 0 s indicates inhale onset. Black outlines indicate statistically significant clusters (FDR corrected $P < 0.05$). The subject-averaged respiratory signal is overlaid (black line). (B) Enlarged versions of the dashed-lined windows in panel A. (C) Individual maximal ITPC values in panel B. ITPC was higher in the anticipatory condition compared to the nonanticipatory condition (two-tailed paired *t* test; $T_{12} = 3.62$, $P = 0.0035$). (D) Individual maximal ITPC values across each half window in panel B. Peak ITPC values are plotted for each participant, for each time window, for each condition. An ANOVA analysis found a significant main effect of "anticipatory-state" ($F_{1,12} = 12.53$, $P = 0.0041$) and a significant interaction between "time-window" and "anticipatory-state" ($F_{1,12} = 13.56$, $P = 0.0031$). ITPC was significantly larger during the anticipatory condition compared to the nonanticipatory condition in the later time interval ($T_{12} = 4.09$, $P = 0.0015$) but not in the earlier time interval ($T_{12} = 1.56$, $P = 0.15$). (E) Phase reset was specific to piriform cortex. The ITPC was higher for electrodes located inside piriform cortex compared to those located outside of piriform cortex but on the same depth wire (two-tailed paired *t* test; $T_{12} = 2.37$, $P = 0.035$). The brain image on the left is a representative participant. The bar plot on the right shows the average ITPC for each subject in the time window from −0.5 s to 0 s pre-inhale onset and the frequency range from 0.5 Hz to 2 Hz. PC, piriform cortex; R, right hemisphere. Each colored dot represents one participant in panels C–E. The source data are available at https://github.com/zelanolab/PhaseResettingInOlfactoryAnticipation.git. FDR, false discovery rate; ITPC, intertrial phase coherence.

https://doi.org/10.1371/journal.pbio.3000724.g002

participants' maximal ITPC values within the anticipatory condition only, occurring within the two distinct time intervals (Fig 2D). In a two-tailed paired *t* test with multiple comparisons corrected using the Bonferroni method, we found that the maximal ITPC was significantly stronger in the time interval from [−0.5 s, 0 s], indicating that, in the anticipatory condition only, ITPC became significantly stronger 0.5 s prior to inhale onset (two-tailed paired *t* test, $T_{12} = 5.2$, $P = 0.00022$). Notably, in contrast, there was no significant ITPC difference between
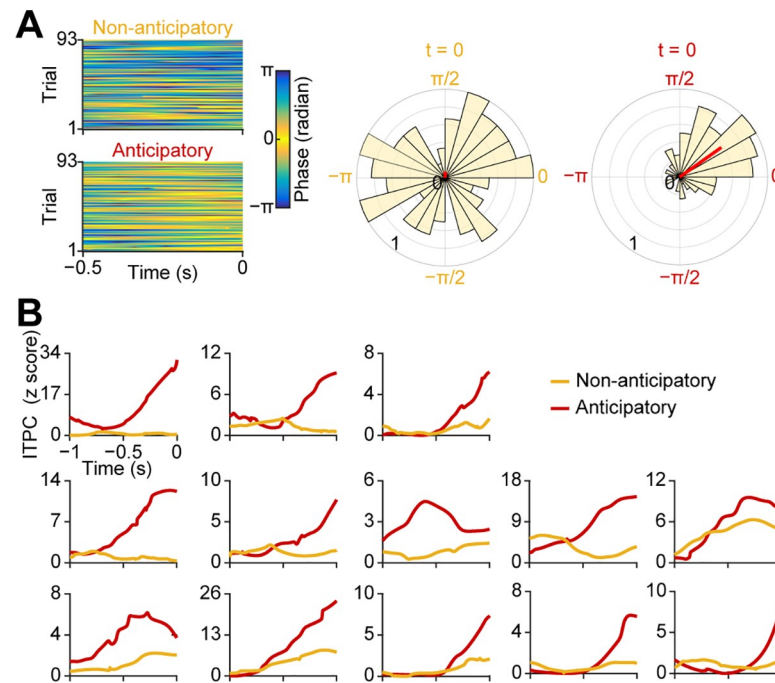
Fig 3. Individual anticipatory phase resets prior to inhale onset. (A) Single-trial instantaneous phase time series (0–2 Hz) for each condition from a representative participant. The raw instantaneous phase over time of the half second prior to inhale (−0.5 s to 0 s) is plotted onto the color map. Each row is a single trial. Increased ITPC is evident in the anticipatory condition as a more skewed color distribution (in the "yellow direction") compared to the nonanticipatory condition. Corresponding rose plots show the normalized distribution of single-trial phases at the inhale onset (t = 0 s) for each condition. The length of the red line on the rose plots indicates the magnitude of the ITPC for each condition. (B) Time course of phase resetting in the pre-inhale time window. For each participant, the Rayleigh z-score of the ITPC (at the maximal frequency from 0.5–2 Hz for each individual) time series is plotted over the 1 s pre-onset time window for each condition. The source data can be found at https://github.com/zelanolab/PhaseResettingInOlfactoryAnticipation.git. ITPC, intertrial phase coherence.

https://doi.org/10.1371/journal.pbio.3000724.g003

the two time intervals for the nonanticipatory condition (two-tailed paired *t* test, $T_{12} = 0.83$, $P = 0.42$). We also computed the averaged time series of ITPC over the entire pre-inhale time window for each individual participant. The increase in ITPC was evident beginning around 0.5 s prior to inhale onset in each individual (Fig 3A and 3B). Taken together, these findings indicate that anticipation resets the phase of ongoing neuronal oscillations in human piriform cortex just before stimulus arrival.

Anticipation does not modulate the power of human piriform oscillations

Phase and power are mathematically independent variables, but ITPC measures can be sensitive to power modulations, which can impact the precision of phase estimates [98,99]. Therefore, in order to test whether differences in power between experimental conditions affected measured differences in ITPC between experimental conditions in our data, we conducted a series of analyses designed to quantify relationships between power and ITPC during the pre-inhale time window. First, we determined whether there were any gross differences in pre-inhale power spectral density (PSD) across conditions. We computed the PSD (from 0–200 Hz, using Matlab's *pwelch.m* function) for each participant for each condition during the pre-inhale time window. We found no significant differences in PSD across conditions during the pre-inhale time window (FDR corrected T-statistics, $P > 0.05$; Fig 4A). Of note, in human piriform cortex we did not see an obvious PSD theta peak, which has been consistently found in
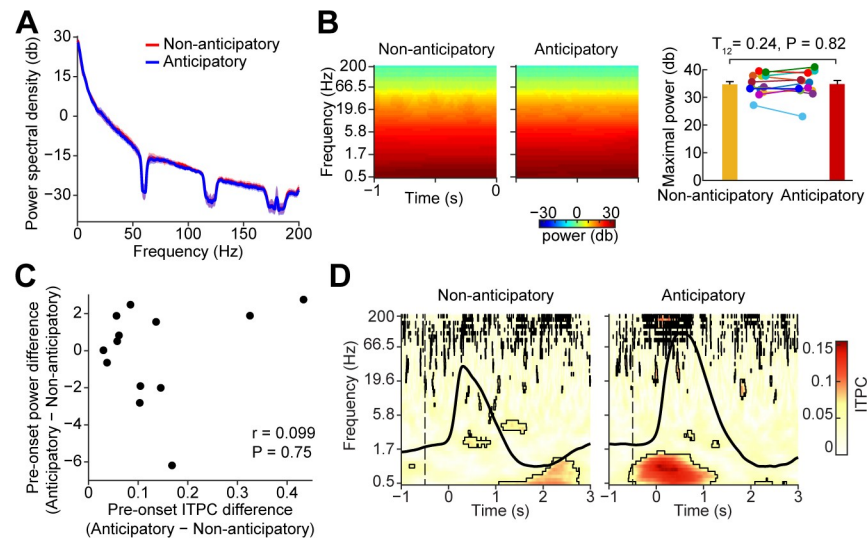
Fig 4. Anticipatory phase reset is not related to pre-inhale power. (A) PSD of the pre-inhale time window. The average PSD is plotted for each condition. The shaded area indicates standard error over participants ($N = 13$). PSD did not differ across conditions (FDR corrected $P > 0.05$). (B) Pre-inhale time-frequency analysis. Average raw power is plotted as a color map for both conditions (two left panels). The bar plot on the far right shows anticipatory peak power (0.5 Hz–12 Hz, from −1 s to 0 s prior to inhale onset) for both conditions. There was no significant difference across conditions (two-tailed paired t test; $T_{12} = 0.24$, $P = 0.82$). Each colored dot represents data from one participant. (C) Pre-inhale phase reset and pre-inhale power are not correlated. The maximal pre-inhale ITPC and power were calculated over 0.5 Hz to 2 Hz and −0.5 s to 0 s prior to inhale onset. The maximal ITPC difference between anticipatory and nonanticipatory conditions is not correlated to power (Spearman correlation, $r = 0.099$; $P = 0.75$). (D) Related to Fig 2A, time-frequency plot of phase reset using a shorter filter window. The $t = 0$ s indicates inhale onset. Black outlines indicate statistically significant clusters (FDR corrected $P < 0.05$). The subject-averaged respiratory signal is overlaid (black line). The source data are available at https://github.com/zelanolab/PhaseResettingInOlfactoryAnticipation.git. FDR, false discovery rate; ITPC, intertrial phase coherence; PSD, power spectral density.

other medial temporal lobe structures such as the hippocampus [100]. Second, because PSD calculations cannot detect power changes over time, we tested whether any condition-related differences in LFP power arose over the course of the pre-inhale time window. For each individual participant, we conducted a Hilbert-based time-frequency analysis of the instantaneous power over frequencies from 0.5 Hz to 200 Hz during the 1 s time window prior to inhale onset. In this analysis, baseline correction can impact signal-to-noise ratio, which impacts ITPC [99]; therefore, we conducted this analysis using raw data without baseline correction. We found no significant differences in power across conditions during the pre-inhale time window (FDR corrected $P > 0.05$, Fig 4B). This was true both in a combined analysis, including trials across all subjects (Fig 4B, left), and in an individual analysis in each subject (Fig 4B, right, bar plot; two-tailed paired t test; $T_{12} = 0.24$, $P = 0.82$). Third, even though we found no differences in LFP power across conditions using the PSD or Hilbert measures, it was still possible that small changes in power across conditions could impact differences in the strength of ITPC across subjects. We therefore looked for a relationship between pre-inhale ITPC and differences in pre-inhale power across conditions across subjects. We found no relationship between these measures in either the 0.5 Hz to 2 Hz or 0.5 Hz to 8 Hz frequency ranges (Fig 4C; frequency range of 0.5–2 Hz: Spearman correlation, $r = 0.0099$, $P = 0.75$; Pearson correlation, $r = 0.22$, $P = 0.48$; frequency range of 0.5–8 Hz: Spearman correlation, $r = 0.27$, $P = 0.37$; Pearson correlation, $r = 0.25$, $P = 0.42$). Finally, it is possible that "temporal leakage" due to inherent temporal smoothing during filtering could have caused poststimulus effects to impact

measures in the prestimulus time window. To control for this possibility, we reran our time-frequency analysis using a shorter filter window (2 cycles per frequency) [101]. Virtually identical results were found using the shorter window length (Fig 4D), confirming that our findings were not due to filter smearing effects.

Combined, these findings suggest that increases in ITPC during odor anticipation are independent of differences in power, and therefore reflect true phase resetting.

Anticipatory phase reset correlates with odor-evoked responses

Anticipation enhances perception. We hypothesized that if phase resetting is a neural signature of anticipation, then it should relate to odor coding and perceptual accuracy. Therefore, we next looked for relationships between pre-inhale ITPC and measures—both neural and behavioral—of olfactory perception following odor presentation.

Odor-evoked theta-band responses in human piriform cortex may carry odor-identity information [102] and appear to play an important role in odor coding in rodents [68,103,104]. Based on these findings, we reasoned that if anticipatory phase resetting is related to odor coding, then it should predict ensuing odor-induced theta power. To test this hypothesis, we looked for a relationship between the pre-inhale ITPC and the postinhale increase in power between conditions. We first established that odor-induced theta power following inhale onset was stronger in the anticipatory compared to the nonanticipatory condition (Fig 5A and 5B). We found that theta power was significantly increased during anticipatory trials compared to nonanticipatory trials in both a combined analysis and in each individual participant (combined analysis: FDR corrected $P < 0.05$; individual analysis: two-tailed paired t test; $T_{12} = 5.68$, $P = 0.000102$). We then asked whether odor-evoked theta power increases were related to anticipatory phase resetting. To do this, we looked for a predictive relationship between the pre-inhale ITPC and the postinhale theta power increase across subjects. We found a robust positive correlation between the strength of ITPC during anticipation, and odor-induced theta power increases across subjects (Spearman correlation, r = 0.76, $P = 0.0036$; Fig 5C). This finding suggests that phase resetting of ongoing LFP oscillations prior to the arrival of anticipated odor impacts subsequent processing of that odor. Notably, the observed odor-evoked increase in theta power in the olfactory anticipation condition could be explained by the consistent delta phase reset and phase amplitude coupling. Thus, although a clear relationship was found between anticipatory signatures and subsequent odor processing, the oscillatory mechanism underlying this subsequent odor processing cannot be definitively determined by our data.

Anticipation-induced phase reset improves olfactory perceptual accuracy

If anticipation matters for odor perception, then it should impact behavioral outcomes. Therefore, we conducted two separate analyses that were each designed to look for a relationship between pre-inhale phase reset and perceptual accuracy on the ensuing task. To do this, given the relatively small number of incorrect trials per subject, and the fact that ITPC measures stabilize at around 20 to 30 trials [98], we used a single-trial measure of ITPC: the deviation from the mean phase (DMP) measure [105,106]. DMP provides an estimate of how well each trial aligns to the clustered phase angle, thus constituting a single-trial measure of phase resetting. In this analysis, for a given trial, a small DMP value would indicate the presence of phase reset, whereas a large DMP value would indicate a lack of phase reset. First, for each participant, we grouped trials according to their perceptual accuracy (correct or incorrect) and then examined the DMP for each group. Second, for each participant, we grouped trials according to their DMP (well-aligned versus poorly aligned) and then examined the perceptual accuracy for each
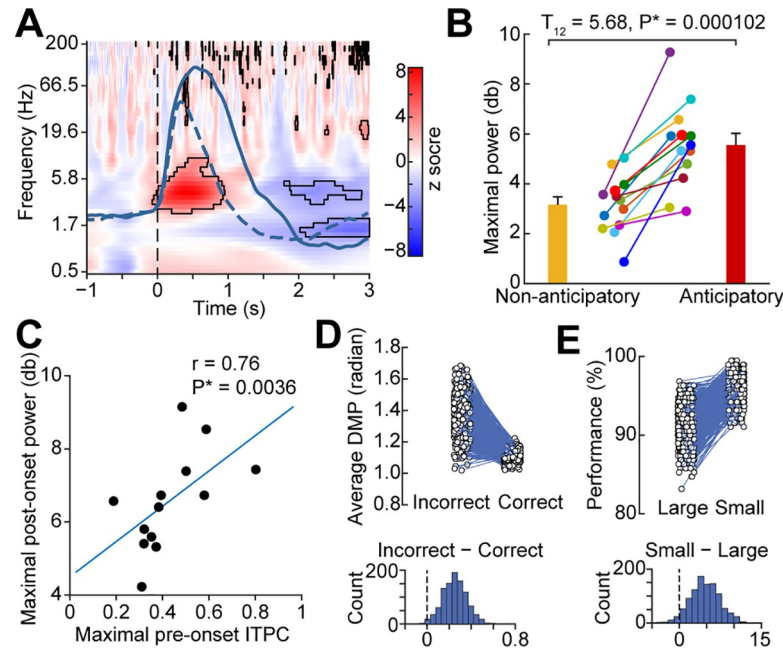
Fig 5. Anticipatory phase reset correlates with odor-induced theta power and olfactory perceptual accuracy. (A) Anticipation prior to inhale increases theta power following inhale. The difference in power across conditions is shown. Black outlines indicate statistically significant differences (permutation test, FDR corrected $P < 0.05$). The vertical dotted line indicates inhale onset, and solid and dashed overlays indicate subject-averaged respiratory signals for anticipatory and nonanticipatory conditions respectively. (B) Anticipation-induced theta power increases are evident in each individual participant. The maximal power over the frequency range 0.5 Hz to 12 Hz and 0 s to 1 s following inhale onset is plotted for each participant. Anticipatory power is greater than nonanticipatory power across participants (two-tailed paired t test, $T_{12} = 5.68$, $P = 0.000102$). Each colored dot represents data from one participant. (C) Anticipatory phase reset prior to inhale onset correlates with odor-evoked theta power across subjects. The maximal ITPC from −0.5 s to 0 s pre-inhale and 0.5 Hz to 2 Hz for each participant is plotted against the maximal theta power following inhale onset for each participant. A significant correlation was evident (Spearman correlation, $r = 0.76$, $P = 0.0036$). Each dot indicates one participant. (D) Single-trial phase resetting prior to inhale onset predicts olfactory perceptual accuracy. The DMP is plotted for correct and incorrect trials computed on each repetition ($N = 1,000$) of a bootstrap analysis (upper panel). Each dot is the DMP value for each condition for that repetition, with lines connecting the values obtained on each repetition. The distribution of the difference is plotted (lower panel), which was statistically compared to zero. Correct trials were more closely aligned to the mean phase than incorrect trials, indicating stronger phase resetting prior to inhale on trials when the participant later made an accurate olfactory perceptual decision (percentage-based $P = 0.009$; sign-test $P = 2.72 \times 10^{-211}$). (E) Single-trial phase resetting predicts olfactory perceptual accuracy. The behavioral accuracy is plotted for trials with small and large pre-inhale DMP values, computed on each repetition ($N = 1,000$) of a bootstrap analysis (upper panel). Each dot is the accuracy for each condition for that repetition, with lines connecting the values obtained on each repetition. The distribution of the difference is plotted (lower panel), which was statistically compared to zero. Trials with small DMP values resulted in higher accuracy on the task than those with large DMP values, indicating that stronger phase resetting occurred prior to inhale on trials when the participant later made an accurate olfactory perceptual decision (percentage-based $P = 0.042$; sign-test $P = 3.66 \times 10^{-191}$). The source data are available at https://github.com/zelanolab/PhaseResettingInOlfactoryAnticipation.git. DMP, deviation from the mean phase; FDR, false discovery rate; ITPC, intertrial phase coherence.

https://doi.org/10.1371/journal.pbio.3000724.g005

group. For both analyses, bootstrapped distributions of difference values were computed across conditions, the mean of which was subsequently compared to zero (Fig 5D and 5E). In our first analysis, we found that correct trials had smaller pre-inhale DMP values compared to incorrect trials (making no assumption of a normal distribution, 991 out of 1,000 repetitions yielded a difference > 0, $P = 0.009$; if we assume a normal distribution, $Z = 2.3$, $P = 0.01$; paired t test, $T_{999} = 72.58$ $P = 0$; sign-test $P = 2.72 \times 10^{-211}$), suggesting better alignment with the mean phase for correct over incorrect trials (Fig 5D). In our second analysis, we found that trials with small pre-inhale DMP had better ensuing perceptual accuracy compared to trials with

large pre-inhale DMP ([Fig 5E](#); making no assumption of a normal distribution, 958 out of 1,000 repetitions yielded a difference > 0, $P = 0.04$; if we assume a normal distribution, $Z = 1.8$, $P = 0.03$; paired t test, $T_{999} = 57.31$, $P = 0$; sign-test $P = 3.66 \times 10^{-191}$). Thus, results of these two complementary analyses suggest that anticipatory phase resetting in piriform cortex improves perceptual accuracy.

Anticipatory phase reset does not correlate with olfactory motor behavior

Anticipation induces activation of motor and premotor areas prior to arrival of a stimulus, likely in preparation for movement relevant to the expected stimulus [107–111]. In line with this, anticipation of odor has been shown to impact both olfactory perception (behavior and coding) [64,66,112,113] and olfactory sampling (sniffing/motor) behavior [52,114]. It is therefore possible that anticipatory phase resetting in piriform cortex relates to both olfactory perception and olfactory motor behavior. In the previous section, we established a link between anticipatory pre-inhale phase resetting and olfactory perceptual responses. To determine whether this link was specific to perceptual effects of anticipation and not confounded by olfactory motor responses, we next asked whether there was also a link between anticipatory phase resets and subsequent olfactory motor behavior. To do this, we looked for a predictive relationship between prestimulus ITPC and the ensuing inhale peak and duration, both across and within subjects.

First, we examined the respiratory signal of each subject following inhale onset for anticipatory and nonanticipatory conditions separately ([Fig 6A](#)). Confirming findings from previous studies, we found that inhale peaks and durations were significantly larger following inhale onset for the anticipatory compared to the nonanticipatory condition (Peak value: two-tailed paired t test, $T_{12} = 9.04$, $P = 1.05 \times 10^{-6}$; [Fig 6B](#), left. Inhale duration: two-tailed paired t test, $T_{12} = 5.34$, $P = 0.00018$; [Fig 6B](#), right), suggesting a link between olfactory anticipation and olfactory motor behavior. However, it does not necessarily follow from this finding that there is a link between anticipatory phase resetting and olfactory motor behavior. To address this possibility, we asked whether the strength of the pre-inhale ITPC predicted the size of the ensuing inhale; if true, this would suggest a link between pre-inhale phase resetting and motor-related anticipatory correlates. We computed the difference in ITPC between anticipatory and nonanticipatory conditions and compared this to the difference in inhale peak value between the two conditions across participants. We found no statistically significant correlation between pre-inhale ITPC increase prior to inhale onset and ensuing inhale peak (Spearman correlation, $r = 0.15$, $P = 0.63$; Pearson correlation, $r = 0.4$, $P = 0.15$) or inhale duration (Spearman correlation, $r = 0.011$, $P = 0.98$; Pearson correlation, $r = -0.24$, $P = 0.44$; [Fig 6C](#)). However, the lack of a significant correlation across subjects did not rule out the possibility of effects within subjects. To confirm the across-subject findings at a within-subjects level, we next used a median split of the DMP to separate each subject's trials into groups of well-aligned (small DMP) and poorly aligned (large DMP) phase at onset. We then compared the inhale sizes for the trials from each group. We found no relationship between the degree of phase alignment at inhale onset and the size of the ensuing inhale at the individual level ([Fig 6D](#)). These findings suggest that increased phase resetting during anticipation of odor does not impact respiratory behavior and is therefore unlikely to relate to the motor component of olfactory anticipation.

Discussion

In this study, we found that anticipation of odor resets the phase of low-frequency LFP oscillations in piriform cortex prior to inhale onset. The strength of this phase reset was positively
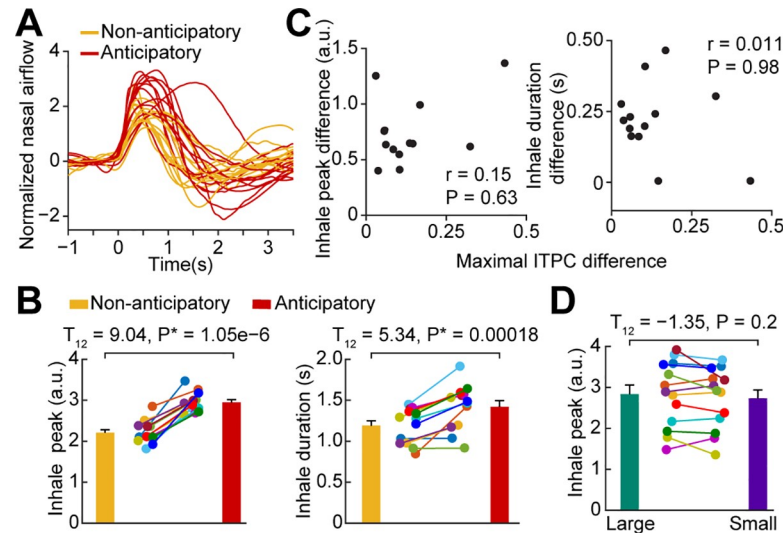
Fig 6. Anticipatory phase reset does not relate to subsequent olfactory motor behavior. (A) Average respiratory signals for each participant; anticipatory (red) and nonanticipatory (yellow) conditions. (B) Inhale peaks and durations. Each colored dot represents data from one participant. The anticipatory condition had both higher inhale peaks (left, $T_{12} = 9.04$, $P = 1.05 \times 10^{-6}$) and longer durations (right, $T_{12} = 5.34$, $P = 0.00018$) compared to nonanticipatory condition. Statistics were performed using a two-tailed paired t test. (C) Anticipatory phase resetting is not correlated to changes in olfactory motor behavior across subjects. Each colored dot represents data from one participant. No significant correlation was found between pre-inhale ITPC and subsequent inhale peaks (Spearman correlation, r = 0.15, $P = 0.63$; Pearson correlation, r = 0.42, $P = 0.15$) or durations (Spearman correlation, r = 0.011, $P = 0.98$; Pearson correlation, r = −0.24, $P = 0.44$). (D) Anticipatory phase resetting is not correlated to changes in olfactory motor behavior within subjects. For each subject, we computed inhale peaks for trials median split by small and large DMP values. We found that trials with poor phase alignment had inhale peaks similar to those in trials with good phase alignment (two-tailed paired t test, $T_{12} = -1.35$, $P = 0.2$). Each colored dot represents data from one participant. The source data are available at https://github.com/zelanolab/PhaseResettingInOlfactoryAnticipation.git. a.u., arbitrary units; DMP, deviation from the mean phase; ITPC, intertrial phase coherence.

https://doi.org/10.1371/journal.pbio.3000724.g006

correlated with anticipation-induced increases in odor response magnitude but not with anticipation-induced increases in inhale size. We also found that anticipatory phase reset improves olfactory perceptual accuracy. Together, these findings suggest that anticipation may enhance olfactory perception through neural dynamics that result in resetting of LFP phase to the timing of stimulus arrival. Notably, we did not observe changes in oscillatory power during olfactory anticipation, highlighting the importance of oscillatory phase dynamics over power modulations in olfactory anticipation. Because LFP oscillations represent rhythmic increases and decreases in neuronal excitability [30,115], our results suggest that olfactory anticipation may bring LFP oscillations to an optimal phase at the time of odor arrival (in this case, the onset of nasal inhalation). This study was limited to a focus on the oscillatory dynamics of low-frequency (delta) oscillations in piriform cortex. Future studies are needed to characterize the impacts of anticipatory—or nonanticipatory—states on higher frequency ranges.

Compared to other sensory systems, neural signatures of olfactory anticipation are less understood. In the visual and auditory systems, it is well established that phase reset of ongoing LFPs occurs during anticipation, which is linked to improved perception [20–36,40–46]. Here, we established that anticipatory phase reset occurs in the olfactory system, despite its distinct paleocortical architecture and its lack of a precortical thalamic relay. Our study extends findings from previous fMRI studies on human olfactory attention showing that BOLD activity in piriform cortex is modulated by attention to odor, during both anticipatory and poststimulus attentional periods [52,59–61]. Because fMRI is not a direct measure of neural activity, our finds suggest that the observed anticipatory phase shift may be detectable (indirectly) by fMRI

techniques. Furthermore, multivariate analysis methods have shown that spatial patterns of activity in piriform cortex during odor anticipation are stimulus-specific, representing the particular odor being anticipated [64]. However, a limitation of BOLD signal is its poor temporal resolution, which precludes analysis of oscillatory and phase dynamics of LFP oscillations. Our use of iEEG methods overcame these limitations, allowing us to measure LFP oscillations directly from human piriform cortex and to show that oscillatory phase, but not power, is modulated by anticipation of odor. Although iEEG methods have excellent temporal precision, they have limited spatial coverage; thus, future studies using both fMRI and iEEG techniques in the same participant pool would provide a powerful tool for measurement of both LFPs and multivariate spatial patterns and allow for a thorough investigation of the spatial extent of anticipatory effects across the many regions of primary olfactory cortex. For example, a recent study in rodents found olfactory attentional effects in the olfactory tubercle [116], from which we were not able to record in this study. Furthermore, a recent study reported modulations of the timing of transitions between metastable states during gustatory expectation [117], indicating that future work on metastability in human olfactory cortex is needed.

In interpreting our results, there is potential for confusion over the words "expectation" and "anticipation," which are sometimes used interchangeably. Here, we use the terms "anticipation" and "anticipatory" to mean the general belief, prior to inhalation, that odor will be present on the next inhale, without expectations about specific identity or characteristics of the odor and without regard to any reward/punishment. Referring to "expectation(s)" about a coming odor may imply that the subject holds a belief or set of beliefs about characteristics or context of the coming stimulus (for example, labeling of the same chemical as either "cheese" or "vomit" influences olfactory perception of that chemical). Expectations about a coming odor have been shown to impact perception [118–124]. This is distinct from general anticipation of an odor, without beliefs about the characteristics of that odor. In addition, the study of reward anticipation following a stimulus [67,125–127] is also distinct from our use of "anticipation," here, where we consider general anticipation of odor.

Our findings dovetail with current theories of predictive coding, which suggest that top-down influences convey predictive signals at lower frequencies compared to bottom-up signals, which convey prediction errors at higher frequencies [128–133]. We found that the phase of low-frequency oscillations was reset during anticipation, prior to stimulus arrival. Though predictive coding studies have found top-down signals represented in beta-range oscillations [134–137], our results, in keeping with other studies [21,32,35,39,95], found anticipatory phase resetting in delta range oscillations. Previous studies have shown that prediction-related neural signals carry feature-specific information across modalities [64,138–142]. In our study, participants were told that an odor was coming, but they did not receive information that could be used to predict its identity. Thus, our study examined the state of general olfactory anticipation, analogous to general anticipation of tastes that have been studied in rodent gustatory cortex [6,117]. While predictive coding may involve multivariate spatial patterns of activity prior to the arrival of a stimulus [64,143–145], our data suggest these patterns may be combined with shifts in the phase of ongoing LFPs. Additional studies on olfactory anticipation will clarify these remaining questions.

A prominent idea is that sensory cortex oscillations entrain with rhythmic stimuli, especially during sustained attention [42–44,146]. When stimuli are not rhythmic, or during inattentive states, cortical oscillations are decoupled from stimuli and are characterized by different oscillatory properties. However, how this idea would apply to the olfactory system, where the stimuli are odor chemicals which lack inherent temporal structure, is unclear [147]. Here, we show that in human olfaction, low-frequency oscillations align with the timing of

stimulus onset by synchronizing with inhalation. In this way, anticipatory mechanisms in the olfactory system may involve oscillatory synchrony between respiration—which controls the timing of stimulus arrival—and cortex, analogous to the mechanism underlying entrainment between rhythmic stimuli and cortex in vision and audition. This suggests that there is a yet-to-be-discovered olfactory "unattended state," even though the olfactory system is, notably, never decoupled from respiratory rhythms [89]. We hypothesize that olfactory unattended states involve changes in higher frequency oscillations, as observed in vision and audition [147–149].

Methods

Ethics statement

The study was approved by the Institutional Review Boards of Northwestern University, University of Chicago, and Stanford University, and the study adhered to the declaration of Helsinki. Written informed consent was obtained from all participants.

Participants

Our study included iEEG data sets from 13 participants with medication-resistant epilepsy. All participants had depth electrodes implanted stereotactically for clinical presurgical evaluation (Table 1 and Fig 1A). Electrode locations were determined solely based on clinical need and, in our participant population, included piriform cortex and amygdala within the medial temporal lobe. Data were acquired at Northwestern Memorial Hospital (10 participants), University of Chicago (2 participants), and Stanford University (1 participant).

Subjects participated in olfactory tasks that involved periodic presentation of cued odors with time periods between odor trials exceeding 6 times the respiratory period of the individual. During this intertrial period, subjects breathed naturally through the nose and no odor was anticipated or presented. In each case, the task included an olfactory perceptual behavioral component. Each data set included respiratory data that was of consistent high quality both during and between trials. The experimental tasks were conducted in each participant's hospital room and were computer-controlled, presented to subjects using an Apple laptop computer running Matlab (RRID: SCR_001622) via the PsychToolBox extension (RRID: SCR_002881). Synchronization TTL pulses were delivered to the clinical EEG acquisition system using a data acquisition board (USB-1208FS, Measurement Computing) to mark task events, including participant responses. Odors were delivered either manually using squeeze-bottles or automatically using a 12-channel computer-controlled olfactometer. Seven of the participants performed an odor detection task in which they were presented with either odorized or odorless air following a visual cue and were asked to indicate whether an odor was present (S1 Fig). Six participants performed an odor identification task in which they were presented with an odor following a verbal cue and were asked to indicate whether the odor matched the cue. In all cases, trials were separated by approximately 15 to 20 s of natural, unattended breathing of odorless air. Importantly, during these intertrial periods, participants did not anticipate receiving an odor, and no odor was ever delivered during this time. Our analyses were focused on the period occurring immediately prior to inhale onset, during a natural pause in breathing, and thus prior to any potentially confounding effects of sniffing or odor. Notably, all analyses were performed at both the group and the individual level.

Table 1. Demographic and clinical characteristics of patients.

Patient	Gender	Age (years)	Age of seizure onset (years)	Epileptogenic zone	Medial temporal lobe coverage	Brain MRI	Site
1	Female	61	35	Left temporo-occipital lobe	Right and left	Remote prior left posterior parietal craniotomy, with cystic encephalomalacia and gliosis; gliosis in left parahippocampal gyrus and left middle/inferior temporal white matter	NU
2	Female	46	16	Right mesial temporal lobe	Right	Right mesial temporal sclerosis	UC
3	Female	23	20	Right temporo-parietal lobe	Right	Nodular foci (2) along lateral right temporal horn periventricular white matter	NU
4	Female	27	13	Temporal lobe	Right	Small nonspecific foci of hyperintense T2FLAIR in bilateral frontal lobe white matter and left parietal white matter	NU
5	Female	28	20	Right fronto-temporal lobe	Right	Small cavernous malformation in right medial orbital gyrus and left superior temporal gyrus; meningioma in anterior interhemispheric falx and focal cortical enhancement in left temporo-occipital region and pons	NU
6	Female	28	13	Left temporal lobe	Right and left	Normal	SU
7	Male	20	15	Left mesial temporal lobe	Right and left	Normal	UC
8	Male	34	28	Right mesial temporal lobe	Right	Normal	NU
9	Male	32	22	Left basal temporal lobe	Left	Normal	NU
10	Female	27	22	Left mesial temporal lobe	Left	Left mesial temporal sclerosis	NU
11	Female	29	22	Left temporal lobe	Left	Normal	NU
12	Female	36	<1	Left mesial temporal	Left	Left mesial temporal sclerosis	NU
13	Female	25	3	Left mesial temporal	Left	Normal	NU

Abbreviations: NU, Northwestern University; SU, Stanford University; UC, University of Chicago

Respiratory and iEEG recordings

iEEG data were acquired using the clinical 128-channel EEG recording system (Nihon Kohden, Tokyo, Japan) in place at Northwestern Memorial Hospital and Stanford University Medical Center, and a clinical 256-channel EEG recording system (Natus Medical Incorporated, Pleasanton, CA) at University of Chicago Medical Center. The sampling rate for each participant was determined clinically and ranged from 500 Hz to 2000 Hz across participants. The reference and ground consisted of surgically implanted electrode strips on the surface of the brain facing towards the scalp. Depth macro-electrodes used at Northwestern University and University of Chicago were manufactured by Integra (Plainsboro, New Jersey), and depth macro-electrodes used at Sandford University were manufactured by Ad-Tech (Racine, Wisconsin).

Respiratory data were recorded using a piezoelectric pressure transducer (Salter Labs Model #5500) attached to a nasal cannula. These data were recorded by the clinical acquisition system and were therefore automatically synchronized with the iEEG data. Of note, the data acquisition system imposes a hardware high-pass filter of 0.08 Hz.

Electrode localization

Depth electrodes were localized using pre-operative structural magnetic resonance imaging (MRI) scans and postoperative computed tomography (CT) scans using FSL's registration tool

flirt (FMRIB Software Library, RRID: SCR_002823) [150,151]. Individual CT images were registered to MRI images using a degree of freedom of 6, with a cost function of mutual information, which was followed by a 12 degree-of-freedom affine registration. Individual MRI images were registered to a Montreal Neurological Institute (MNI) standard brain (MNI152_1mm_-brain) with a degree of freedom of 12. The transformation matrices generated above were combined to create a transformation from the individual CT image to standard MNI space. The electrodes were localized by thresholding the raw CT image and calculating the unweighted mass center of each electrode. Finally, the coordinates were converted to standard MNI space using the transformation matrix generated above (Fig 1A).

Phase resetting analysis (ITPC)

We used ITPC to estimate phase resetting in piriform cortex. ITPC provides an estimate of the consistency of the instantaneous phase across trials, aligned to an event, and ranges in value from 0 to 1, where 0 indicates no phase clustering, and 1 indicates perfect phase clustering [97].

Combined ITPC analysis

iEEG data were down-sampled to 500 Hz and re-referenced to a common average. In preparation for the combined analysis, iEEG time series were normalized for each subject by subtracting the average of the time series and dividing by the standard deviation. The resulting normalized time series were then band-pass filtered at 50 log-spaced frequencies between 0.5 Hz and 200 Hz (Fig 2A), with the bandwidth logarithmically increasing from 1 Hz to 2 Hz. The signal was filtered using a two-pass, zero-phase finite impulse response filter as implemented by *fieldtrip* (RRID: SCR_004849). Subsequently, the Hilbert transform was applied to the band-pass filtered signal in order to extract the instantaneous phase of each time point and each frequency bin. The resulting phase time-series was segmented into inhale-onset-aligned epochs going from 1 s prior to, to 3 s following, the onset of the inhale. This was performed for all inhales over the course of the experiments, thus encompassing both anticipatory and nonanticipatory inhales. Because there were a larger number of nonanticipatory inhales between trials than anticipatory inhales during trials, we analyzed a subset of nonanticipatory breaths consisting of the same number as that of anticipatory trials performed for each subject. This was achieved by selecting a random subset of all nonanticipatory trials for each subject. The resulting trials were pooled over all subjects, resulting in 891 anticipatory trials and 891 nonanticipatory trials (Fig 2). The difference in ITPC value was calculated across trials at each time-frequency point, for each condition separately, using the Phase-Locking-Value index across trials [97]. The statistical significance of the ITPC for each condition was evaluated with the Rayleigh test. Multiple comparisons were corrected using the FDR method on the *P* values obtained from the Rayleigh tests.

Individual participant ITPC analysis

To compute the ITPC for each individual participant, we followed the same steps as described above for the combined analysis, using the trials for that individual only. We then computed the maximal ITPC for each individual in the frequency range from 0.5 Hz to 2 Hz, and the time range from −1 s to 0 s (Fig 2C), or −1 s to −0.5 s and −0.5 s to 0 s (Fig 2D), for each condition. Statistical significance was determined using ANOVAs and paired *t* tests across participants.

Pre-inhale power analyses

Power Spectral Density: PSD was computed using Matlab's *pwelch* function over the frequency range from 0 Hz to 200 Hz, with a step size of 0.05 Hz. This was computed over the entire pre-inhale time window from −1 s to 0 s. PSD was calculated separately for each participant and for each condition. The resulting PSD values were then converted to decibels, averaged across participants, and plotted, along with the standard error, across subjects (Fig 4A). Statistics were computed using paired *t* tests and FDR correction for multiple comparisons.

Time-frequency analysis of pre-inhale power: For each participant separately, iEEG data were filtered at 50 log-spaced frequencies between 0.5 Hz and 200 Hz, with the bandwidth logarithmically increasing from 1 Hz to 2 Hz. The signal was filtered using a two-pass, zero-phase finite impulse response filter as implemented by *fieldtrip*. The Hilbert transform was then applied to the band-pass-filtered signal in order to extract the instantaneous amplitude of each time point and each frequency bin. The resulting amplitude-time series were then temporally smoothed with a moving average filter kernel of 10 ms. To evaluate event-related power changes, the amplitude-time series were segmented into inhale-onset-aligned epochs going from −1 s to 0 s (at inhale onset) for each condition. Epochs were converted to power by squaring the amplitude values. The power spectrogram of each condition was separately calculated by averaging the corresponding power epochs across trials at each frequency. Then, decibel transformation was applied to the averaged spectrograms. Importantly, for this analysis, no baseline correction was performed. Raw power was used in order to avoid potentially confounding effects of baseline correction: baseline correction modifies signal-to-noise ratios, which can impact the accuracy of phase estimates [99]. This resulted in spectrograms of anticipatory and nonanticipatory conditions in the pre-inhale time window for each subject. The resulting individual-participant spectrograms were then averaged across participants. Statistics were performed using paired *t* tests across participants and FDR correction for multiple comparisons (Fig 4B, left). To confirm these findings at the individual level, we also show the maximal power for each participant across 0.5 Hz to 2 Hz and −1 s to 0 s (inhale onset) for each condition and computed a paired *t* test across participants (Fig 4B, right).

To estimate the correlation between pre-inhale ITPC and pre-inhale power, we computed the difference in maximal power across conditions for each participant and the difference in maximal ITPC across conditions for each participant. The Spearman r value was computed using Matlab's *corrcoef* function. Pearson correlation values were also computed, with no difference in results. This analysis was also conducted over a broader frequency range, 0.5 Hz to 8 Hz, with no difference in results (Fig 4C).

Postinhale power analyses

iEEG data were preprocessed and band-pass filtered as described earlier. The Hilbert transform was applied to the band-pass-filtered signal in order to extract the instantaneous amplitude of each time point and each frequency bin. The resulting amplitude-time series were then temporally smoothed with a moving average filter kernel of 10 ms.

To evaluate event-related power changes (Fig 5A), the amplitude-time series were segmented into sniff-onset-aligned epochs going from 1 s prior to, to 3 s following, the inhale, for all anticipatory and nonanticipatory trials for each subject. All sniff-aligned epochs were converted to power by squaring the values. The power spectrogram of each condition was separately calculated by averaging the corresponding power epochs across trials at each frequency. Then, decibel transformation was applied to the averaged spectrograms, which was further normalized by subtracting a common baseline average. The baseline was defined as the time window of one second prior to the inhale onset. Finally, the power difference between

anticipatory and nonanticipatory conditions was calculated by subtracting the baseline-corrected nonanticipatory power from the baseline-corrected anticipatory power.

The statistical significance of the power change for each condition was determined using nonparametric permutation testing [152]. Surrogate events were generated by shifting actual events by a random amount. The average power across these permuted events was calculated for each permutation. A distribution of surrogate values was obtained by repeating this procedure 1,000 times. A z-score map of the actual spectrogram and its corresponding P values was obtained by subtracting the average of the surrogate data and dividing the result by the standard deviation of the surrogate distribution. Multiple comparisons were corrected using the FDR method on the P values obtained.

To perform statistics on the power difference between anticipatory and nonanticipatory conditions, we used a permutation method, in which condition labels were shuffled, and the power difference computed, at each iteration. This procedure was repeated 1,000 times to build a distribution of surrogate values of power differences at each time-frequency point across conditions. A z-score map of the actual power differences and their corresponding P values was obtained by subtracting the average of the surrogate data and dividing the result by the standard deviation of the surrogate distribution. Subsequently, multiple comparisons were corrected using the FDR method.

We also computed the postinhale power for each condition at the individual-participant level, using a paired t test for statistical comparison. For each participant, we computed the maximal power over 0.5 Hz to 12 Hz and over the time range from 0 s to 1 s postinhale. The maximal postinhale power occurred within this time and frequency window for all participants. This was done for each participant, for each condition, and statistical comparisons were conducted using a paired t test across participants (Fig 5B).

Linking phase resetting and olfactory perceptual accuracy

We performed two analyses to explore the impact of phase resetting on olfactory perceptual accuracy. Given the relatively small number of incorrect trials per subject and the fact that ITPC measures stabilize at around 20 to 30 trials [98], we made use of a single-trial measure of ITPC—the DMP [105,106]. DMP is a single-trial measure of the extent of phase reset relative to the mean phase of the ITPC. Our two analyses involved first grouping trials according to their accuracy (correct or incorrect) and then computing the DMP of each group; and, second, grouping trials according to their DMP (small or large) and then computing the accuracy of each group. DMP was computed according to methods in the work by Hanslmayr and colleagues [105]. The ITPC across correct and incorrect trials was calculated for each participant. To compute the DMP of each trial for each participant, we first determined the frequency at which the maximal ITPC occurred at inhale onset. Next, the distance between the phase angle of each trial and the mean phase angle was calculated at onset (t = 0 s) using *circ_dist* as implemented in CircStat Matlab toolbox (RRID: SCR_016651). After computing phase distances for each trial for each participant, values were combined across subjects. For both analyses, bootstrapping was performed with 1,000 repetitions.

In the first analysis, for each subject whose performance on the task included both correct and incorrect trials, we grouped trials according to their accuracy (correct versus incorrect). Trials were then grouped across all subjects into two vectors (correct and incorrect). DMP values were determined using individual subject ITPC phase angles (at time 0 s and the frequency at which each individual's ITPC was maximal), and the resulting DMP values were combined across subjects for each group (correct and incorrect). This resulted in a list of DMP values for each trial, for each group (correct and incorrect). For each bootstrap repetition (N = 1,000), a

subset of trials from each group was randomly selected using the *randi* function in Matlab (with replacement), and the average DMP was computed for both subsets. The difference between the DMP average for correct trials and that for incorrect trials was calculated. This yielded a distribution (N = 1,000) of the difference between DMP values for trials that had been grouped solely by their accuracy, with no a priori information about their DMP values (Fig 5D). Statistics were computed both under no assumption of a normal distribution and under assumption of a normal distribution. Specifically, making no assumption about the characteristics of the distribution, we computed the percentage of values in the distribution that fell above zero and computed the P value from that [98]. Assuming a normal distribution, we computed z-score from the mean and standard deviation of the distribution and converted those into P values [98]. Finally, we also computed the P value using Matlab's *signtest* and a paired *t* test.

In the second analysis, we did the opposite: That is, we grouped trials initially by DMP values and then calculated the accuracy of each group. Trials were randomly selected as described in the first analysis above. On each bootstrap repetition, for each subject, the DMP was calculated for each trial as described above. Values were combined across participants and sorted from small to large. Then, we separated the DMP values into well-aligned and poorly aligned groups by taking the smallest 20% for the well-aligned group (closest to the mean phase) and the largest 20% for the poorly aligned group (farthest from the mean phase) (Fig 5E). The performance in each group was then calculated as percentage of correct trials over all trials. Statistics were conducted exactly as described for the first analysis above.

Linking phase reset and olfactory motor behavior

To analyze the respiratory signals for each subject, we first normalized the data by subtracting the mean and dividing by the standard deviation of the entire respiratory signal (Fig 6). For each subject, inhale durations were computed as the time between inhale onset and the first zero-crossing. The peaks were computed as the maximum airflow value over the duration of inhale. To perform analysis on the respiratory data at the individual level, we used the DMP measure to estimate single-trial phase resets (using the same procedure and parameters as described above) and then determined whether these phase resets related to inhale sizes. DMP was computed for each trial for each participant. We then defined well-aligned and poorly aligned trials using a median split and computed inhale peaks for each trial type. Statistics were performed using a paired *t* test across participants.

Supporting information

S1 Fig. Experimental paradigms. Related to Fig 1. Following selection of data sets according to our inclusion criteria (described in detail in the main text), data from two olfactory tasks were included. In a detection task (top panel), the participants were presented with either odorized or odorless air following a visual cue and indicated whether an odor was present via button press. In an identification task (bottom panel), the participants were presented with an odor following an auditory cue and indicated whether the odor matched the cue via button press. The red outlined area (box just prior to inhale onset) indicates the time window of interest in our analyses, specifically, the pre-inhale anticipatory period.
(TIF)

Acknowledgments

Author Contributions

Conceptualization: Ghazaleh Arabkheradmand, Guangyu Zhou, Torben Noto, Qiaohan Yang, Gregory Lane, Christina Zelano.

Data curation: Gregory Lane, Christina Zelano.

Formal analysis: Ghazaleh Arabkheradmand, Guangyu Zhou, Christina Zelano.

Funding acquisition: Christina Zelano.

Methodology: Ghazaleh Arabkheradmand, Guangyu Zhou, Joshua M. Rosenow, Gregory Lane, Christina Zelano.

Resources: Stephan U. Schuele, Josef Parvizi, Jay A. Gottfried, Shasha Wu, Joshua M. Rosenow, Mohamad Z. Koubeissi.

Software: Ghazaleh Arabkheradmand, Guangyu Zhou.

Supervision: Guangyu Zhou, Gregory Lane, Christina Zelano.

Visualization: Ghazaleh Arabkheradmand, Guangyu Zhou, Gregory Lane, Christina Zelano.

Writing – original draft: Ghazaleh Arabkheradmand, Guangyu Zhou, Gregory Lane, Christina Zelano.

Writing – review & editing: Guangyu Zhou, Torben Noto, Qiaohan Yang, Jay A. Gottfried, Gregory Lane, Christina Zelano.

References

1. Engel AK, Fries P, Singer W. Dynamic predictions: oscillations and synchrony in top-down processing. Nat Rev Neurosci. 2001; 2: 704–716. https://doi.org/10.1038/35094565 PMID: 11584308

2. Jaramillo S, Zador AM. The auditory cortex mediates the perceptual effects of acoustic temporal expectation. Nat Neurosci. 2011; 14: 246–251. https://doi.org/10.1038/nn.2688 PMID: 21170056

3. Doherty JR, Rao A, Mesulam MM, Nobre AC. Synergistic effect of combined temporal and spatial expectations on visual attention. J Neurosci. 2005; 25: 8259–8266. https://doi.org/10.1523/JNEUROSCI.1821-05.2005 PMID: 16148233

4. Gilbert CD, Sigman M. Brain states: top-down influences in sensory processing. Neuron. 2007; 54: 677–696. https://doi.org/10.1016/j.neuron.2007.05.019 PMID: 17553419

5. Veldhuizen MG, Bender G, Constable RT, Small DM. Trying to detect taste in a tasteless solution: modulation of early gustatory cortex by attention to taste. Chem Senses. 2007; 32: 569–581. https://doi.org/10.1093/chemse/bjm025 PMID: 17495173

6. Samuelsen CL, Gardner MPH, Fontanini A. Effects of cue-triggered expectation on cortical processing of taste. Neuron. 2012; 74: 410–422. https://doi.org/10.1016/j.neuron.2012.02.031 PMID: 22542192

7. Iemi L, Busch NA, Laudini A, Haegens S, Samaha J, Villringer A, et al. Multiple mechanisms link presti-mulus neural oscillations to sensory responses. Elife. 2019; 8: e43620. https://doi.org/10.7554/eLife.43620 PMID: 31188126

8. Watrous AJ, Miller J, Qasim SE, Fried I, Jacobs J. Phase-tuned neuronal firing encodes human con-textual representations for navigational goals. Elife. 2018; 7: e32554. https://doi.org/10.7554/eLife.32554 PMID: 29932417

9. Sela L, Sobel N. Human olfaction: a constant state of change-blindness. Exp Brain Res. 2010; 205: 13–29. https://doi.org/10.1007/s00221-010-2348-6 PMID: 20603708

10. Snyder AC, Yu BM, Smith MA. Distinct population codes for attention in the absence and presence of visual stimulation. Nat Commun. 2018; 9: 4382. https://doi.org/10.1038/s41467-018-06754-5 PMID: 30348942

11. Luck SJ, Chelazzi L, Hillyard SA, Desimone R. Neural mechanisms of spatial selective attention in areas V1, V2, and V4 of macaque visual cortex. J Neurophysiol. 1997; 77: 24–42. https://doi.org/10.1152/jn.1997.77.1.24 PMID: 9120566

12. Reynolds JH, Pasternak T, Desimone R. Attention increases sensitivity of V4 neurons. Neuron. 2000; 26: 703–714. https://doi.org/10.1016/s0896-6273(00)81206-4 PMID: 10896165

13. Lee J, Williford T, Maunsell JHR. Spatial attention and the latency of neuronal responses in macaque area V4. J Neurosci. 2007; 27: 9632–9637. https://doi.org/10.1523/JNEUROSCI.2734-07.2007 PMID: 17804623

14. Williford T, Maunsell JHR. Effects of spatial attention on contrast response functions in macaque area V4. J Neurophysiol. 2006; 96: 40–54. https://doi.org/10.1152/jn.01207.2005 PMID: 16772516

15. Boynton GM. A framework for describing the effects of attention on visual responses. Vision Res. 2009; 49: 1129–1143. https://doi.org/10.1016/j.visres.2008.11.001 PMID: 19038281

16. Luo TZ, Maunsell JHR. Neuronal modulations in visual cortex are associated with only one of multiple components of attention. Neuron. 2015; 86: 1182–1188. https://doi.org/10.1016/j.neuron.2015.05.007 PMID: 26050038

17. Kastner S, Pinsk MA, De Weerd P, Desimone R, Ungerleider LG. Increased activity in human visual cortex during directed attention in the absence of visual stimulation. Neuron. 1999; 22: 751–761. https://doi.org/10.1016/s0896-6273(00)80734-5 PMID: 10230795

18. Ress D, Backus BT, Heeger DJ. Activity in primary visual cortex predicts performance in a visual detection task. Nat Neurosci. 2000; 3: 940–945. https://doi.org/10.1038/78856 PMID: 10966626

19. Foxe JJ, Snyder AC. The role of alpha-band brain oscillations as a sensory suppression mechanism during selective attention. Front Psychol. 2011; 2: 154. https://doi.org/10.3389/fpsyg.2011.00154 PMID: 21779269

20. Lakatos P, Shah AS, Knuth KH, Ulbert I, Karmos G, Schroeder CE. An oscillatory hierarchy controlling neuronal excitability and stimulus processing in the auditory cortex. J Neurophysiol. 2005; 94: 1904–1911. https://doi.org/10.1152/jn.00263.2005 PMID: 15901760

21. Lakatos P, Karmos G, Mehta AD, Ulbert I, Schroeder CE. Entrainment of neuronal oscillations as a mechanism of attentional selection. Science. 2008; 320: 110–113. https://doi.org/10.1126/science.1154735 PMID: 18388295

22. Hanslmayr S, Volberg G, Wimber M, Dalal SS, Greenlee MW. Prestimulus oscillatory phase at 7 Hz gates cortical information flow and visual perception. Curr Biol. 2013; 23: 2273–2278. https://doi.org/10.1016/j.cub.2013.09.020 PMID: 24184106

23. Jansen BH, Brandt ME. The effect of the phase of prestimulus alpha activity on the averaged visual evoked response. Electroencephalogr Clin Neurophysiol. 1991; 80: 241–250. https://doi.org/10.1016/0168-5597(91)90107-9 PMID: 1713834

24. Gruber WR, Zauner A, Lechinger J, Schabus M, Kutil R, Klimesch W. Alpha phase, temporal attention, and the generation of early event related potentials. Neuroimage. 2014; 103: 119–129. https://doi.org/10.1016/j.neuroimage.2014.08.055 PMID: 25219334

25. Klimesch W, Sauseng P, Hanslmayr S. EEG alpha oscillations: the inhibition–timing hypothesis. Brain Res Rev. 2007; 53: 63–88. https://doi.org/10.1016/j.brainresrev.2006.06.003 PMID: 16887192

26. Jensen O, Gips B, Bergmann TO, Bonnefond M. Temporal coding organized by coupled alpha and gamma oscillations prioritize visual processing. Trends Neurosci. 2014; 37: 357–369. https://doi.org/10.1016/j.tins.2014.04.001 PMID: 24836381

27. Haegens S, Nácher V, Luna R, Romo R, Jensen O. α-Oscillations in the monkey sensorimotor network influence discrimination performance by rhythmical inhibition of neuronal spiking. Proc Natl Acad Sci U S A. 2011; 108: 19377–19382. https://doi.org/10.1073/pnas.1117190108 PMID: 22084106

28. Haegens S, Barczak A, Musacchia G, Lipton ML, Mehta AD, Lakatos P, et al. Laminar profile and physiology of the rhythm in primary visual, auditory, and somatosensory regions of neocortex. J Neurosci. 2015; 35: 14341–14352. https://doi.org/10.1523/JNEUROSCI.0600-15.2015 PMID: 26490871

29. Jones MR, Boltz M. Dynamic attending and responses to time. Psychol Rev. 1989; 96: 459–491. https://doi.org/10.1037/0033-295x.96.3.459 PMID: 2756068

30. Schroeder CE, Lakatos P. Low-frequency neuronal oscillations as instruments of sensory selection. Trends Neurosci. 2009; 32: 9–18. https://doi.org/10.1016/j.tins.2008.09.012 PMID: 19012975

31. Henry MJ, Obleser J. Frequency modulation entrains slow neural oscillations and optimizes human listening behavior. Proc Natl Acad Sci U S A. 2012; 109: 20095–20100. https://doi.org/10.1073/pnas.1213390109 PMID: 23151506

32. Stefanics G, Hangya B, Hernádi I, Winkler I, Lakatos P, Ulbert I. Phase entrainment of human delta oscillations can mediate the effects of expectation on reaction speed. J Neurosci. 2010; 30: 13578–13585. https://doi.org/10.1523/JNEUROSCI.0703-10.2010 PMID: 20943899

33. Praamstra P, Kourtis D, Kwok HF, Oostenveld R. Neurophysiology of implicit timing in serial choice reaction-time performance. J Neurosci. 2006; 26: 5448–5455. https://doi.org/10.1523/JNEUROSCI.0440-06.2006 PMID: 16707797

34. Mathewson KE, Gratton G, Fabiani M, Beck DM, Ro T. To see or not to see: prestimulus α phase predicts visual awareness. J Neurosci. 2009; 29: 2725–2732. https://doi.org/10.1523/JNEUROSCI.3963-08.2009 PMID: 19261866

35. Cravo AM, Rohenkohl G, Wyart V, Nobre AC. Temporal expectation enhances contrast sensitivity by phase entrainment of low-frequency oscillations in visual cortex. J Neurosci. 2013; 33: 4002–4010. https://doi.org/10.1523/JNEUROSCI.4675-12.2013 PMID: 23447609

36. Miniussi C, Wilding EL, Coull JT, Nobre AC. Orienting attention in time. Brain. 1999; 122: 1507–1518. https://doi.org/10.1093/brain/122.8.1507 PMID: 10430834

37. Helfrich RF, Fiebelkorn IC, Szczepanski SM, Lin JJ, Parvizi J, Knight RT, et al. Neural mechanisms of sustained attention are rhythmic. Neuron. 2018; 99: 854–865.e5. https://doi.org/10.1016/j.neuron.2018.07.032 PMID: 30138591

38. Vanrullen R. Visual attention: a rhythmic process? Curr Biol. 2013; 23: R1110–R1112. https://doi.org/10.1016/j.cub.2013.11.006 PMID: 24355791

39. Breska A, Deouell LY. Neural mechanisms of rhythm-based temporal prediction: delta phase-locking reflects temporal predictability but not rhythmic entrainment. PLoS Biol. 2017; 15: e2001665. https://doi.org/10.1371/journal.pbio.2001665 PMID: 28187128

40. Rohenkohl G, Nobre AC. Alpha oscillations related to anticipatory attention follow temporal expectations. J Neurosci. 2011; 31: 14076–14084. https://doi.org/10.1523/JNEUROSCI.3387-11.2011 PMID: 21976492

41. Busch NA, Dubois J, VanRullen R. The phase of ongoing EEG oscillations predicts visual perception. J Neurosci. 2009; 29: 7869–7876. https://doi.org/10.1523/JNEUROSCI.0113-09.2009 PMID: 19535598

42. Dugué L, Marque P, VanRullen R. The phase of ongoing oscillations mediates the causal relation between brain excitation and visual perception. J Neurosci. 2011; 31: 11889–11893. https://doi.org/10.1523/JNEUROSCI.1161-11.2011 PMID: 21849549

43. Busch NA, VanRullen R. Spontaneous EEG oscillations reveal periodic sampling of visual attention. Proc Natl Acad Sci U S A. 2010; 107: 16048–16053. https://doi.org/10.1073/pnas.1004801107 PMID: 20805482

44. Vanrullen R, Busch NA, Drewes J, Dubois J. Ongoing EEG phase as a trial-by-trial predictor of perceptual and attentional variability. Front Psychol. 2011; 2: 60. https://doi.org/10.3389/fpsyg.2011.00060 PMID: 21716580

45. Callaway E, Yeager CL. Relationship between reaction time and electroencephalographic alpha phase. Science (80-). 1960; 132: 1765–1766. https://doi.org/10.1126/science.132.3441.1765 PMID: 13689987

46. Drewes J, VanRullen R. This is the rhythm of your eyes: the phase of ongoing electroencephalogram oscillations modulates saccadic reaction time. J Neurosci. 2011; 31: 4698–4708. https://doi.org/10.1523/JNEUROSCI.4795-10.2011 PMID: 21430168

47. Fritz JB, Elhilali M, David S V., Shamma SA. Auditory attention—focusing the searchlight on sound. Curr Opin Neurobiol. 2007; 17: 437–455. https://doi.org/10.1016/j.conb.2007.07.011 PMID: 17714933

48. Kanwisher N, Wojciulik E. Visual attention: insights from brain imaging. Nat Rev Neurosci. 2000; 1: 91–100. https://doi.org/10.1038/35039043 PMID: 11252779

49. Knudsen EI. Fundamental components of attention. Annu Rev Neurosci. 2007; 30: 57–78. https://doi.org/10.1146/annurev.neuro.30.051606.094256 PMID: 17417935

50. Knudsen EI. Neural circuits that mediate selective attention: a comparative perspective. Trends Neurosci. 2018; 41: 789–805. https://doi.org/10.1016/j.tins.2018.06.006 PMID: 30075867

51. Gregoriou GG, Gotts SJ, Zhou H, Desimone R. Long-range neural coupling through synchronization with attention. Prog Brain Res. 2009; 176: 35–45. https://doi.org/10.1016/S0079-6123(09)17603-3 PMID: 19733748

52. Plailly J, Howard JD, Gitelman DR, Gottfried JA. Attention to odor modulates thalamocortical connectivity in the human brain. J Neurosci. 2008; 28: 5257–5267. https://doi.org/10.1523/JNEUROSCI.5607-07.2008 PMID: 18480282

53. Spence C, Ketenmann B, Kobal G, McGlone FP. Selective attention to the chemosensory modality. Percept Psychophys. 2000; 62: 1265–1271. https://doi.org/10.3758/bf03212128 PMID: 11019622

54. Spence C, McGlone FP, Ketenmann B, Kobal G. Attention to olfaction. A psychophysical investigation. Exp Brain Res. 2001; 138: 432–437. https://doi.org/10.1007/s002210100713 PMID: 11465740

55. Pause BM, Sojka B, Ferstl R. Central processing of odor concentration is a temporal phenomenon as revealed by chemosensory event-related potentials (CSERP). Chem Senses. 1997; 22: 9–26. https://doi.org/10.1093/chemse/22.1.9 PMID: 9056082

56. Krauel K, Pause BM, Sojka B, Schott P, Ferstl R. Attentional modulation of central odor processing. Chem Senses. 1998; 23: 423–432. https://doi.org/10.1093/chemse/23.4.423 PMID: 9759529

57. Geisler MW, Murphy C. Event-related brain potentials to attended and ignored olfactory and trigeminal stimuli. Int J Psychophysiol. 2000; 37: 309–315. https://doi.org/10.1016/s0167-8760(00)00111-2 PMID: 10858576

58. Morgan CD, Murphy C. Differential effects of active attention and age on event-related potentials to visual and olfactory stimuli. Int J Psychophysiol. 2010; 78: 190–199. https://doi.org/10.1016/j.ijpsycho.2010.07.008 PMID: 20688110

59. Sabri M, Radnovich AJ, Li TQ, Kareken DA. Neural correlates of olfactory change detection. Neuro-image. 2005; 25: 969–974. https://doi.org/10.1016/j.neuroimage.2004.12.033 PMID: 15808997

60. Zelano C, Bensafi M, Porter J, Mainland J, Johnson B, Bremner E, et al. Attentional modulation in human primary olfactory cortex. Nat Neurosci. 2005; 8: 114–120. https://doi.org/10.1038/nn1368 PMID: 15608635

61. Rolls ET, Grabenhorst F, Margot C, da Silva MA, Velazco MI. Selective attention to affective value alters how the brain processes olfactory stimuli. J Cogn Neurosci. 2008; 20: 1815–1826. https://doi.org/10.1162/jocn.2008.20128 PMID: 18370603

62. Singh AK, Touhara K, Okamoto M. Electrophysiological correlates of top-down attentional modulation in olfaction. Sci Rep. 2019; 9: 4953. https://doi.org/10.1038/s41598-019-41319-6 PMID: 30894641

63. De Araujo IE, Rolls ET, Velazco MI, Margot C, Cayeux I. Cognitive modulation of olfactory processing. Neuron. 2005; 46: 671–679. https://doi.org/10.1016/j.neuron.2005.04.021 PMID: 15944134

64. Zelano C, Mohanty A, Gottfried JA. Olfactory predictive codes and stimulus templates in piriform cortex. Neuron. 2011; 72: 178–187. https://doi.org/10.1016/j.neuron.2011.08.010 PMID: 21982378

65. Macrides F, Eichenbaum HB, Forbes WB. Temporal relationship between sniffing and the limbic theta rhythm during odor discrimination reversal learning. J Neurosci. 1982; 2: 1705–1717. https://doi.org/10.1523/JNEUROSCI.02-12-01705.1982 PMID: 7143047

66. Carlson KS, Gadziola MA, Dauster ES, Wesson DW. Selective attention controls olfactory decisions and the neural encoding of odors. Curr Biol. 2018; 28: 2195–2205.e4. https://doi.org/10.1016/j.cub.2018.05.011 PMID: 30056854

67. Kepecs A, Uchida N, Mainen ZF. Rapid and precise control of sniffing during olfactory discrimination in rats. J Neurophysiol. 2007; 98: 205–213. https://doi.org/10.1152/jn.00071.2007 PMID: 17460109

68. Kay LM, Beshel J, Brea J, Martin C, Rojas-Líbano D, Kopell N. Olfactory oscillations: the what, how and what for. Trends Neurosci. 2009; 32: 207–214. https://doi.org/10.1016/j.tins.2008.11.008 PMID: 19243843

69. Eeckman FH, Freeman WJ. Correlations between unit firing and EEG in the rat olfactory system. Brain Res. 1990; 528: 238–244. https://doi.org/10.1016/0006-8993(90)91663-2 PMID: 2271924

70. Fontanini A, Bower JM. Slow-waves in the olfactory system: an olfactory perspective on cortical rhythms. Trends Neurosci. 2006; 29: 429–437. https://doi.org/10.1016/j.tins.2006.06.013 PMID: 16842864

71. Rojas-Líbano D, Frederick DE, EgaÃ±a JI, Kay LM. The olfactory bulb theta rhythm follows all frequencies of diaphragmatic respiration in the freely behaving rat. Front Behav Neurosci. 2014; 8: 214. https://doi.org/10.3389/fnbeh.2014.00214 PMID: 24966821

72. Li A-A, Gong L, Liu Q, Li X, Xu F. State-dependent coherences between the olfactory bulbs for delta and theta oscillations. Neurosci Lett. 2010; 480: 44–48. https://doi.org/10.1016/j.neulet.2010.05.093 PMID: 20594948

73. Fontanini A, Spano P, Bower JM. Ketamine-xylazine-induced slow (<1.5 Hz) oscillations in the rat piriform (olfactory) cortex are functionally correlated with respiration. J Neurosci. 2003; 23: 7993–8001. https://doi.org/10.1523/JNEUROSCI.23-22-07993.2003 PMID: 12954860

74. Laurent G, Wehr M, Davidowitz H. Temporal representations of odors in an olfactory network. J Neurosci. 1996; 16: 3837–3847. https://doi.org/10.1523/JNEUROSCI.16-12-03837.1996 PMID: 8656278

75. Herrero JL, Khuvis S, Yeagle E, Cerf M, Mehta AD. Breathing above the brain stem: volitional control and attentional modulation in humans. J Neurophysiol. 2018; 119: 145–159. https://doi.org/10.1152/jn.00551.2017 PMID: 28954895

76. Kay LM, Freeman WJ. Bidirectional processing in the olfactory-limbic axis during olfactory behavior. Behav Neurosci. 1998; 112: 541–553. https://doi.org/10.1037//0735-7044.112.3.541 PMID: 9676972

77. Adrian ED. Olfactory reactions in the brain of the hedgehog. J Physiol. 1942; 100: 459–473. https://doi.org/10.1113/jphysiol.1942.sp003955 PMID: 16991539

78. Sem-Jacobsen CW, Bickford RG, Dodge HW, Petersen MC. Human olfactory responses recorded by depth electrography. Proc Staff Meet Mayo Clin. 1953; 28: 166–170. PMID: 13037903

79. Rojas-Líbano D, Kay LM. Olfactory system gamma oscillations: the physiological dissection of a cognitive neural system. Cogn Neurodyn. 2008; 2: 179–194. https://doi.org/10.1007/s11571-008-9053-1 PMID: 19003484

80. Buonviso N, Amat C, Litaudon P, Roux S, Royet J-P, Farget V, et al. Rhythm sequence through the olfactory bulb layers during the time window of a respiratory cycle. Eur J Neurosci. 2003; 17: 1811–1819. https://doi.org/10.1046/j.1460-9568.2003.02619.x PMID: 12752780

81. Cenier T, Amat C, Litaudon P, Garcia S, Lafaye de Micheaux P, Liquet B, et al. Odor vapor pressure and quality modulate local field potential oscillatory patterns in the olfactory bulb of the anesthetized rat. Eur J Neurosci. 2008; 27: 1432–1440. https://doi.org/10.1111/j.1460-9568.2008.06123.x PMID: 18364022

82. Laurent G, Davidowitz H. Encoding of olfactory information with oscillating neural assemblies. Science (80-). 1994; 265: 1872–1875. https://doi.org/10.1126/science.265.5180.1872 PMID: 17797226

83. Carlson KS, Dillione MR, Wesson DW. Odor- and state-dependent olfactory tubercle local field potential dynamics in awake rats. J Neurophysiol. 2014; 111: 2109–2123. https://doi.org/10.1152/jn.00829.2013 PMID: 24598519

84. Ito J, Roy S, Liu Y, Cao Y, Fletcher M, Lu L, et al. Whisker barrel cortex delta oscillations and gamma power in the awake mouse are linked to respiration. Nat Commun. 2014; 5: 3572. https://doi.org/10.1038/ncomms4572 PMID: 24686563

85. Lockmann AL V., Laplagne DA, Tort ABL. Olfactory bulb drives respiration-coupled beta oscillations in the rat hippocampus. Eur J Neurosci. 2018; 48: 2663–2673. https://doi.org/10.1111/ejn.13665 PMID: 28833629

86. Tort ABL, Brankačk J, Draguhn A. Respiration-entrained brain rhythms are global but often overlooked. Trends Neurosci. 2018; 41: 186–197. https://doi.org/10.1016/j.tins.2018.01.007 PMID: 29429805

87. Yanovsky Y, Ciatipis M, Draguhn A, Tort ABL, Brankačk J. Slow oscillations in the mouse hippocampus entrained by nasal respiration. J Neurosci. 2014; 34: 5949–5964. https://doi.org/10.1523/JNEUROSCI.5287-13.2014 PMID: 24760854

88. Jessberger J, Zhong W, Brankačk J, Draguhn A, Draguhn A. Olfactory bulb field potentials and respiration in sleep-wake states of mice. Neural Plast. 2016; 2016: 4570831. https://doi.org/10.1155/2016/4570831 PMID: 27247803

89. Zelano C, Jiang H, Zhou G, Arora N, Schuele S, Rosenow J, et al. Nasal respiration entrains human limbic oscillations and modulates cognitive function. J Neurosci. 2016; 36: 12448–12467. https://doi.org/10.1523/JNEUROSCI.2586-16.2016 PMID: 27927961

90. Fontanini A, Bower JM. Variable coupling between olfactory system activity and respiration in ketamine/xylazine anesthetized rats. J Neurophysiol. 2005; 93: 3573–3581. https://doi.org/10.1152/jn.01320.2004 PMID: 15689385

91. Adrian ED. The electrical activity of the mammalian olfactory bulb. Electroencephalogr Clin Neurophysiol. 1950; 2: 377–388. https://doi.org/10.1016/0013-4694(50)90075-7 PMID: 14793507

92. Liu Y, McAfee SS, Heck DH. Hippocampal sharp-wave ripples in awake mice are entrained by respiration. Sci Rep. 2017; 7: 8950. https://doi.org/10.1038/s41598-017-09511-8 PMID: 28827599

93. Zhong W, Ciatipis M, Wolfenstetter T, Jessberger J, Müller C, Ponsel S, et al. Selective entrainment of gamma subbands by different slow network oscillations. Proc Natl Acad Sci U S A. 2017; 114: 4519–4524. https://doi.org/10.1073/pnas.1617249114 PMID: 28396398

94. Illig KR, Wilson DA. Olfactory Cortex: Comparative Anatomy. 1st ed. In: Kaas J, editor. Encyclopedia of Neuroscience. 1st ed. New York, NY: Elsevier; 2009. pp. 101–106. https://doi.org/10.1016/B978-008045046-9.00971–2

95. Arnal LH, Doelling KB, Poeppel D, C S, AL W, I U, et al. Delta–beta coupled oscillations underlie temporal prediction accuracy. Cereb Cortex. 2015; 25: 3077–3085. https://doi.org/10.1093/cercor/bhu103 PMID: 24846147

96. Tallon-Baudry C, Bertrand O, Delpuech C, Pernier J. Stimulus specificity of phase-locked and non-phase-locked 40 Hz visual responses in human. J Neurosci. 1996; 16: 4240–4249. https://doi.org/10.1523/JNEUROSCI.16-13-04240.1996 PMID: 8753885

97. Lachaux JP, Rodriguez E, Martinerie J, Varela FJ. Measuring phase synchrony in brain signals. Hum Brain Mapp. 1999; 8: 194–208. https://doi.org/10.1002/(sici)1097-0193(1999)8:4<194::aid-hbm4>3.0.co;2-c PMID: 10619414

98. Cohen MX. Analyzing neural time series data: theory and practice. MIT Press. MIT press; 2014. https://doi.org/10.1017/CBO9781107415324.004

99. van Diepen RM, Mazaheri A. The caveats of observing inter-trial phase coherence in cognitive neuroscience. Sci Rep. 2018; 8: 2990. https://doi.org/10.1038/s41598-018-20423-z PMID: 29445210

100. Buzsáki G. Theta oscillations in the hippocampus. Neuron. 2002; 33: 325–340. https://doi.org/10.1016/s0896-6273(02)00586-x PMID: 11832222

101. Wutz A, Weisz N, Braun C, Melcher D. Temporal windows in visual processing: "prestimulus brain state" and "poststimulus phase reset" segregate visual transients on different temporal scales. J Neurosci. 2014; 34: 1554–1565. https://doi.org/10.1523/JNEUROSCI.3187-13.2014 PMID: 24453342

102. Jiang H, Schuele S, Rosenow J, Zelano C, Parvizi J, Tao JX, et al. Theta oscillations rapidly convey odor-specific content in human piriform cortex. Neuron. 2017; 94: 207–219.e4. https://doi.org/10.1016/j.neuron.2017.03.021 PMID: 28384472

103. Kay LM. Theta oscillations and sensorimotor performance. Proc Natl Acad Sci U S A. 2005; 102: 3863–3868. https://doi.org/10.1073/pnas.0407920102 PMID: 15738424

104. Xu W, Wilson DA. Odor-evoked activity in the mouse lateral entorhinal cortex. Neuroscience. 2012; 223: 12–20. https://doi.org/10.1016/j.neuroscience.2012.07.067 PMID: 22871522

105. Hanslmayr S, Aslan A, Staudigl T, Klimesch W, Herrmann CS, Bäuml K-H. Prestimulus oscillations predict visual perception performance between and within subjects. Neuroimage. 2007; 37: 1465–1473. https://doi.org/10.1016/j.neuroimage.2007.07.011 PMID: 17706433

106. Rapela J, Westerfield M, Townsend J. A new foreperiod effect on intertrial phase coherence. Part I: Existence and behavioral relevance. Neural Comput. 2018; 30: 2348–2383. https://doi.org/10.1162/neco_a_01109 PMID: 29949462

107. Riehle A, Requin J. The predictive value for performance speed of preparatory changes in neuronal activity of the monkey motor and premotor cortex. Behav Brain Res. 1993; 53: 35–49. https://doi.org/10.1016/s0166-4328(05)80264-5 PMID: 8466666

108. Vaadia E, Kurata K, Wise SP. Neuronal activity preceding directional and nondirectional cues in the premotor cortex of rhesus monkeys. Somatosens Mot Res. 1988; 6: 207–230. https://doi.org/10.3109/08990228809144674 PMID: 3242346

109. Crammond DJ, Kalaska JF. Prior information in motor and premotor cortex: activity during the delay period and effect on pre-movement activity. J Neurophysiol. 2000; 84: 986–1005. https://doi.org/10.1152/jn.2000.84.2.986 PMID: 10938322

110. Boussaoud D. Attention versus intention in the primate premotor cortex. NeuroImage. Academic Press Inc.; 2001. https://doi.org/10.1006/nimg.2001.0816 PMID: 11373131

111. Bruce CJ, Goldberg ME. Primate frontal eye fields. I. Single neurons discharging before saccades. J Neurophysiol. 1985; 53: 603–635. https://doi.org/10.1152/jn.1985.53.3.603 PMID: 3981231

112. Keller A. Attention and olfactory consciousness. Front Psychol. 2011; 2: 380. https://doi.org/10.3389/fpsyg.2011.00380 PMID: 22203813

113. Laing DG, Glemarec A. Selective attention and the perceptual analysis of odor mixtures. Physiol Behav. 1992; 52: 1047–1053. https://doi.org/10.1016/0031-9384(92)90458-e PMID: 1484860

114. Wesson DW, Donahou TN, Johnson MO, Wachowiak M. Sniffing behavior of mice during performance in odor-guided tasks. Chem Senses. 2008; 33: 581–596. https://doi.org/10.1093/chemse/bjn029 PMID: 18534995

115. Schroeder CE, Lakatos P, Kajikawa Y, Partan S, Puce A. Neuronal oscillations and visual amplification of speech. Trends Cogn Sci. 2008; 12: 106–113. https://doi.org/10.1016/j.tics.2008.01.002 PMID: 18280772

116. Wesson DW, Wilson DA. Sniffing out the contributions of the olfactory tubercle to the sense of smell: hedonics, sensory integration, and more? Neurosci Biobehav Rev. 2011; 35: 655–668. https://doi.org/10.1016/j.neubiorev.2010.08.004 PMID: 20800615

117. Mazzucato L, La Camera G, Fontanini A. Expectation-induced modulation of metastable activity underlies faster coding of sensory stimuli. Nat Neurosci. 2019; 22: 787–796. https://doi.org/10.1038/s41593-019-0364-9 PMID: 30936557

118. Engen T. The effect of expectation on judgments of odor. Acta Psychol (Amst). 1972; 36: 450–458. https://doi.org/10.1016/0001-6918(72)90025-x PMID: 4679755

119. Dubose CN, Cardello A V., Maller O. Effects of colorants and flavorants on identification, perceived flavor intensity, and hedonic quality of fruit-flavored beverage and cake. J Food Sci. 1980; 45: 1393–1399. https://doi.org/10.1111/j.1365-2621.1980.tb06562.x

120. Morrot G, Brochet F, Dubourdieu D. The color of odors. Brain Lang. 2001; 79: 309–320. https://doi.org/10.1006/brln.2001.2493 PMID: 11712849

121. Dalton P. Odor perception and beliefs about risk. Chem Senses. 1996; 21: 447–458. https://doi.org/10.1093/chemse/21.4.447 PMID: 8866108

122. Herz RS, Von Clef J. The influence of verbal labeling on the perception of odors: evidence for olfactory illusions? Perception. 2001; 30: 381–391. https://doi.org/10.1068/p3179 PMID: 11374206

123. Manescu S, Frasnelli J, Lepore F, Djordjevic J. Now you like me, now you don't: Impact of labels on odor perception. Chem Senses. 2014; 39: 167–175. https://doi.org/10.1093/chemse/bjt066 PMID: 24336680

124. Lawless H, Engen T. Associations to odors: Interference, mnemonics, and verbal labeling. J Exp Psychol Hum Learn Mem. 1977; 3: 52–59. https://doi.org/10.1037/0278-7393.3.1.52

125. Zou L quan, Zhou H yu, Zhuang Y, van Hartevelt TJ, Lui SSY, Cheung EFC, et al. Neural responses during the anticipation and receipt of olfactory reward and punishment in human. Neuropsychologia. 2018; 111: 172–179. https://doi.org/10.1016/j.neuropsychologia.2018.02.003 PMID: 29408479

126. Stalnaker TA, Liu TL, Takahashi YK, Schoenbaum G. Orbitofrontal neurons signal reward predictions, not reward prediction errors. Neurobiol Learn Mem. 2018; 153: 137–143. https://doi.org/10.1016/j.nlm.2018.01.013 PMID: 29408053

127. Howard JD, Gottfried JA, Tobler PN, Kahnt T. Identity-specific coding of future rewards in the human orbitofrontal cortex. Proc Natl Acad Sci U S A. 2015; 112: 5195–5200. https://doi.org/10.1073/pnas.1503550112 PMID: 25848032

128. Friston KJ, Bastos AM, Pinotsis D, Litvak V. LFP and oscillations-what do they tell us? Curr Opin Neurobiol. 2015; 31: 1–6. https://doi.org/10.1016/j.conb.2014.05.004 PMID: 25079053

129. Bastos AM, Usrey WM, Adams RA, Mangun GR, Fries P, Friston KJ. Canonical microcircuits for predictive coding. Neuron. 2012; 76: 695–711. https://doi.org/10.1016/j.neuron.2012.10.038 PMID: 23177956

130. Bauer M, Stenner MP, Friston KJ, Dolan RJ. Attentional modulation of alpha/beta and gamma oscillations reflect functionally distinct processes. J Neurosci. 2014; 34: 16117–16125. https://doi.org/10.1523/JNEUROSCI.3474-13.2014 PMID: 25429152

131. Arnal LH, Giraud A-L. Cortical oscillations and sensory predictions. Trends Cogn Sci. 2012; 16: 390–398. https://doi.org/10.1016/j.tics.2012.05.003 PMID: 22682813

132. Recasens M, Gross J, Uhlhaas PJ. Low-frequency oscillatory correlates of auditory predictive processing in cortical-subcortical networks: a MEG-study. Sci Rep. 2018; 8: 14007. https://doi.org/10.1038/s41598-018-32385-3 PMID: 30228366

133. Han B, VanRullen R. The rhythms of predictive coding? Pre-stimulus phase modulates the influence of shape perception on luminance judgments. Sci Rep. 2017; 7: 43573. https://doi.org/10.1038/srep43573 PMID: 28262824

134. Bressler SL, Richter CG. Interareal oscillatory synchronization in top-down neocortical processing. Curr Opin Neurobiol. 2015; 31: 62–66. https://doi.org/10.1016/j.conb.2014.08.010 PMID: 25217807

135. van Pelt S, Heil L, Kwisthout J, Ondobaka S, van Rooij I, Bekkering H, et al. Beta- and gamma-band activity reflect predictive coding in the processing of causal events. Soc Cogn Affect Neurosci. 2016; 11: 973–980. https://doi.org/10.1093/scan/nsw017 PMID: 26873806

136. Cope TE, Sohoglu E, Sedley W, Patterson K, Jones PS, Wiggins J, et al. Evidence for causal top-down frontal contributions to predictive processes in speech perception. Nat Commun. 2017; 8: 2154. https://doi.org/10.1038/s41467-017-01958-7 PMID: 29255275

137. Sedley W, Gander PE, Kumar S, Kovach CK, Oya H, Kawasaki H, et al. Neural signatures of perceptual inference. Elife. 2016; 5: e11476. https://doi.org/10.7554/eLife.11476 PMID: 26949254

138. Demarchi G, Sanchez G, Weisz N. Automatic and feature-specific prediction-related neural activity in the human auditory system. Nat Commun. 2019; 10: 3440. https://doi.org/10.1038/s41467-019-11440-1 PMID: 31371713

139. Kok P, Mostert P, De Lange FP. Prior expectations induce prestimulus sensory templates. Proc Natl Acad Sci U S A. 2017; 114: 10473–10478. https://doi.org/10.1073/pnas.1705652114 PMID: 28900010

140. Brandman T, Peelen M V. Interaction between scene and object processing revealed by human fMRI and MEG decoding. J Neurosci. 2017; 37: 7700–7710. https://doi.org/10.1523/JNEUROSCI.0582-17.2017 PMID: 28687603

141. Gordon N, Koenig-Robert R, Tsuchiya N, Van Boxtel JJA, Hohwy J. Neural markers of predictive coding under perceptual uncertainty revealed with hierarchical frequency tagging. Elife. 2017; 6: e22749. https://doi.org/10.7554/eLife.22749 PMID: 28244874

142. Arnal LH, Wyart V, Giraud AL. Transitions in neural oscillations reflect prediction errors generated in audiovisual speech. Nat Neurosci. 2011; 14: 797–801. https://doi.org/10.1038/nn.2810 PMID: 21552273

143. Friston K. Prediction, perception and agency. Int J Psychophysiol. 2012; 83: 248–252. https://doi.org/10.1016/j.ijpsycho.2011.11.014 PMID: 22178504

144. Summerfield C, Koechlin E. A neural representation of prior information during perceptual inference. Neuron. 2008; 59: 336–347. https://doi.org/10.1016/j.neuron.2008.05.021 PMID: 18667160

145. Chao ZC, Takaura K, Wang L, Fujii N, Dehaene S. Large-scale cortical networks for hierarchical prediction and prediction error in the primate brain. Neuron. 2018; 100: 1252–1266.e3. https://doi.org/10.1016/j.neuron.2018.10.004 PMID: 30482692

146. Zoefel B, VanRullen R. Oscillatory mechanisms of stimulus processing and selection in the visual and auditory systems: state-of-the-art, speculations and suggestions. Front Neurosci. 2017; 11: 296. https://doi.org/10.3389/fnins.2017.00296 PMID: 28603483

147. Lakatos P, Gross J, Thut G. A new unifying account of the roles of neuronal entrainment. Curr Biol. 2019; 29: R890–R905. https://doi.org/10.1016/j.cub.2019.07.075 PMID: 31550478

148. VanRullen R. Perceptual cycles. Trends Cogn Sci. 2016; 20: 723–735. https://doi.org/10.1016/j.tics.2016.07.006 PMID: 27567317

149. Lakatos P, Barczak A, Neymotin SA, McGinnis T, Ross D, Javitt DC, et al. Global dynamics of selective attention and its lapses in primary auditory cortex. Nat Neurosci. 2016; 19: 1707–1717. https://doi.org/10.1038/nn.4386 PMID: 27618311

150. Jenkinson M, Smith S. A global optimisation method for robust affine registration of brain images. Med Image Anal. 2001; 5: 143–156. https://doi.org/10.1016/s1361-8415(01)00036-6 PMID: 11516708

151. Jenkinson M, Bannister P, Brady M, Smith S. Improved optimization for the robust and accurate linear registration and motion correction of brain images. Neuroimage. 2002; 17: 825–841. https://doi.org/10.1016/s1053-8119(02)91132-8 PMID: 12377157

152. Canolty RT, Soltani M, Dalal SS, Edwards E, Dronkers NF, Nagarajan SS, et al. Spatiotemporal dynamics of word processing in the human brain. Front Neurosci. 2007; 1: 185–196. https://doi.org/10.3389/neuro.01.1.1.014.2007 PMID: 18982128